A Sensitivity Approach to Causal Inference Under Limited Overlap

Yuanzhe Ma Hongseok Namkoong

Columbia University

{ym2865, hongseok.namkoong}@columbia.edu

Abstract

Limited overlap between treated and control groups is a key challenge in observational analysis. Standard approaches like trimming importance weights can reduce variance but introduce a fundamental bias. We propose a sensitivity framework for contextualizing findings under limited overlap, where we assess how irregular the outcome function has to be in order for the main finding to be invalidated. Our approach is based on worst-case confidence bounds on the bias introduced by standard trimming practices, under explicit assumptions necessary to extrapolate counterfactual estimates from regions of overlap to those without. Empirically, we demonstrate how our sensitivity framework protects against spurious findings by quantifying uncertainty in regions with limited overlap.

1 Introduction

Observational data is widely utilized when randomized experiments are infeasible or fail to adequately represent target populations. A key challenge in observational analysis is the lack of overlap between treatment and control groups. Even when a nominally large dataset is collected, the effective sample size may be prohibitively small when there is a region with little overlap between treated and control populations. As an example, if the treatment of interest is rarely observed among older citizens, estimating their counterfactual (treated) outcome becomes inherently unreliable. This challenge is further exacerbated in modern operational contexts, where high-dimensional covariate representations [15] increase data sparsity, making causal identification particularly difficult in regions of the covariate space with small effective sample size. Standard inferential methods relying on asymptotic normal approximations tend to fail silently when the effective sample size is limited. Empirically, different observational datasets with lack of overlap may lead to contradictory conclusions on the treatment effects [43, 38, 36, 22, 23].

Theoretically, several authors have quantified how the lack of overlap deteriorates the convergence rates of typical confidence intervals [32, 6, 46, 52, 20, 40, 19, 31, 41]. In particular, Ma and Wang [40] show that in general, the limiting distribution of the inverse probability weighting (IPW) estimator may not be Gaussian, calling into question the validity of standard central limit theorems-based confidence intervals. Practically, limited overlap results in large importance weights in typical estimators, leading to high variances [30, 32]. To stabilize these estimators, researchers have developed various trimming and reweighting methodologies [10, 11, 39, 26, 47], which are commonly applied in fields including economics and biomedical research [35, 18, 13, 16, 49, 44, 17]. Trimming, in particular, has been shown to improve the accuracy of estimators in certain scenarios [9, 51, 37], and has become a standard practice in cases of limited overlap. While these approaches are effective in reducing variance, they change the estimand and introduce biases that are often difficult to quantify.

To illustrate, we consider the following simple example:

Example 1: We illustrate the impact of limited overlap in a problem with one-dimensional covariate $X \sim \mathsf{Uni}[0,1]$. We defer full details of the data-generating process to Section D.1, and

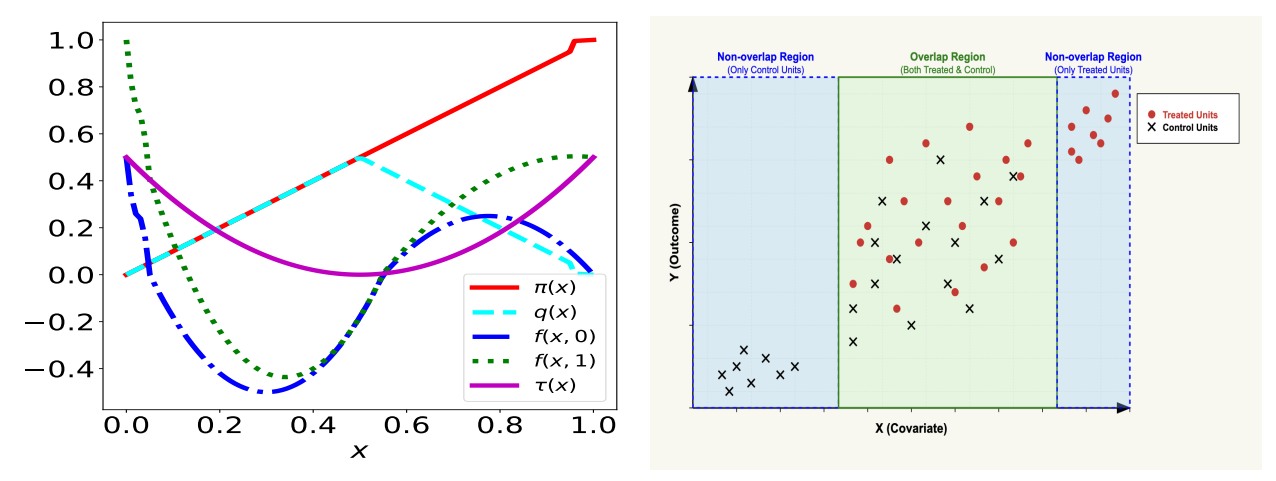


Figure 1. Left: data-generation process used in the simulation setup where $\pi(x) = \mathbb{P}(Z=1 \mid X=x)$ denotes the propensity score, $q(x) = \min\{\pi(x), 1-\pi(x)\}$ measures whether a point has sufficient overlap, and f(x,z) represents the potential outcome for a unit with covariates x under treatment assignment $z \in \{0,1\}$. The individual treatment effect is defined as $\tau(x) = f(x,1) - f(x,0)$. Right: Visualization of one simulated observational dataset.

instead provide a visual illustration in Figure 1. Here, the propensity scores take extreme values when x is close to 0 or 1. In Figure 2a, we observe how the augmented inverse propensity weighting (AIPW) estimator exhibits wide confidence intervals that fluctuate around the true treatment effect, reflecting its instability under limited overlap. To remedy this, we consider standard heuristics that truncate the importance weights based on a threshold from the set

$$\mathcal{E} = \{0.01, 0.02, 0.03, 0.04, 0.05\} \tag{1.1}$$

by selecting ϵ that minimizes the length of the truncated AIPW confidence interval, denoted by AIPW_{partial, ϵ}:

$$\epsilon^{\star} \in \underset{\epsilon \in \mathcal{E}}{\operatorname{argmin}} |\mathsf{AIPW}_{\mathsf{partial},\epsilon}|.$$
 (1.2)

In Figure 2b, we observe AIPW_{partial} gradually deviates from the target estimand as the non-overlap region increases due to the bias introduced by trimming. ⋄

To assess the sensitivity of findings under limited overlap, we propose an inferential method that ensures always-valid uncertainty quantification under explicit assumptions on the smoothness of the outcome function. Unlike asymptotic methods, our approach allows us to quantify instance-specific uncertainty that accurately scales with the level of overlap between the treated and control groups. Consider binary treatments $z_i \in \{0, 1\}$, covariates $x_i \in \mathcal{X}$ and potential outcomes $f(x_i, z_i)$ that generate realized outcome data $y_i = f(x_i, z_i) + \epsilon_i$ for $i = 1, \ldots, n$, where ϵ_i is the noise.

To analyze the bias introduced by truncating based on propensity scores, we allow the modeler to specify a threshold for the *overlap* region (e.g., based on a fitted propensity score), and use S_i to denote the indicator for whether unit i belongs in this region. We separate the average treatment effect into two estimands

$$\tau_{+} := \sum_{i=1}^{n} \mathcal{I}(S_{i} = 1) \frac{1}{n} (f(x_{i}, 1) - f(x_{i}, 0)), \tag{1.3a}$$

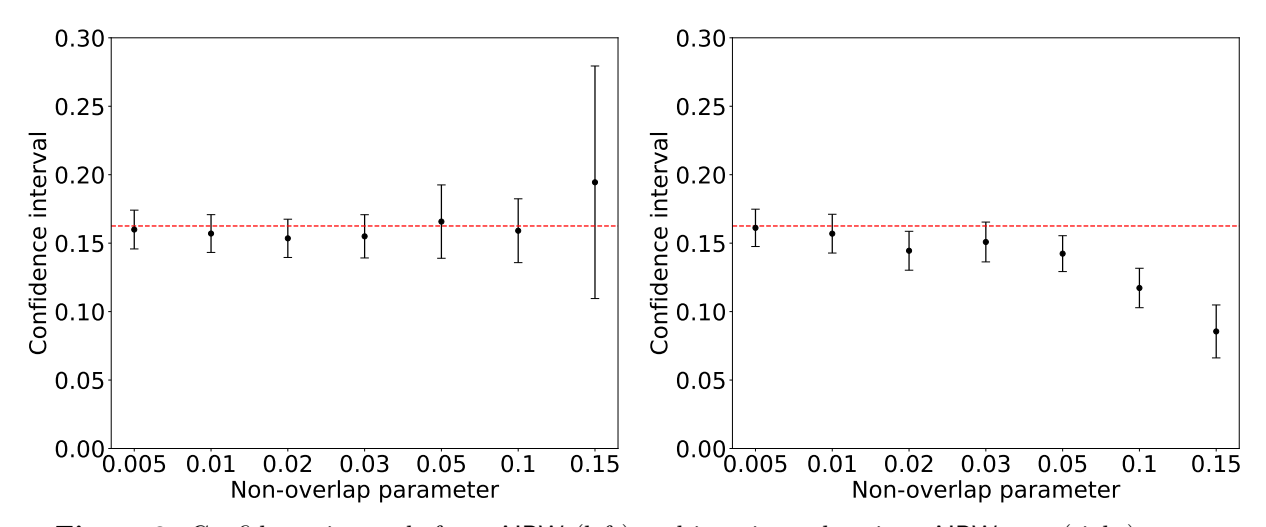


Figure 2. Confidence intervals from AIPW (left) and its trimmed variant AIPW $_{partial}$ (right) across different overlap levels, with the dotted red line representing the true estimand value; higher values on the x-axis mean more limited overlap. **Left**: AIPW yields very wide confidence intervals. **Right**: We follow standard heuristics to truncate data in a way such that AIPW $_{partial}$'s confidence interval has the smallest length.

$$\tau_{-} := \sum_{i=1}^{n} \mathcal{I}(S_{i} = 0) \frac{1}{n} (f(x_{i}, 1) - f(x_{i}, 0)), \tag{1.3b}$$

and assume that standard inferential tools are appropriate for estimating τ_+ .

Since asymptotic normal approximations are invalid in regions with limited overlap, we use a worst-case approach to bound τ_{-} , where we consider all outcome functions that satisfy a smoothness condition. We leverage Donoho [14]'s minimax framework to find the tightest possible confidence interval accounting for the worst-case bias across all admissible outcome functions. Intuitively, this minimax method finds an optimal affine estimator while adding a bias correction term to ensure coverage of the resulting confidence interval.

Armstrong and Kolesár [4] consider the set of Lipschitz outcome functions with smoothness constant L and apply Donoho [14]'s minimax inferential framework to both τ_+ and τ_- , leading to overly conservative confidence intervals. Instead, we only apply the worst-case confidence region over τ_- . Our approach (depicted in Figure 3) separates the estimand to make full use of the standard normal approximation, and only resorts to conservative worst-case bounds when traditional asymptotic assumptions break down. This decomposition allows practitioners to explicitly quantify the potential bias introduced by standard trimming or reweighting practices and understand when their conclusions may be driven by extrapolation beyond well-supported regions.

Instead of requiring the modeler to commit to a particular level of smoothness that is fundamentally untenable, we take a sensitivity analysis perspective where we consider increasing values of L until the confidence bounds cross a certain threshold, and then contextualize this level of smoothness by using data from regions of overlap. This allows us to translate abstract smoothness assumptions into interpretable diagnostics and help analysts validate assumptions necessary for reliable inference when overlap is limited. This form of sensitivity analysis provides a continuous view on model sensitivity, rather than a binary accept/reject judgment. Ultimately, this enables more informed decisions about whether to trust, adjust, or reinterpret conclusions drawn from trimmed

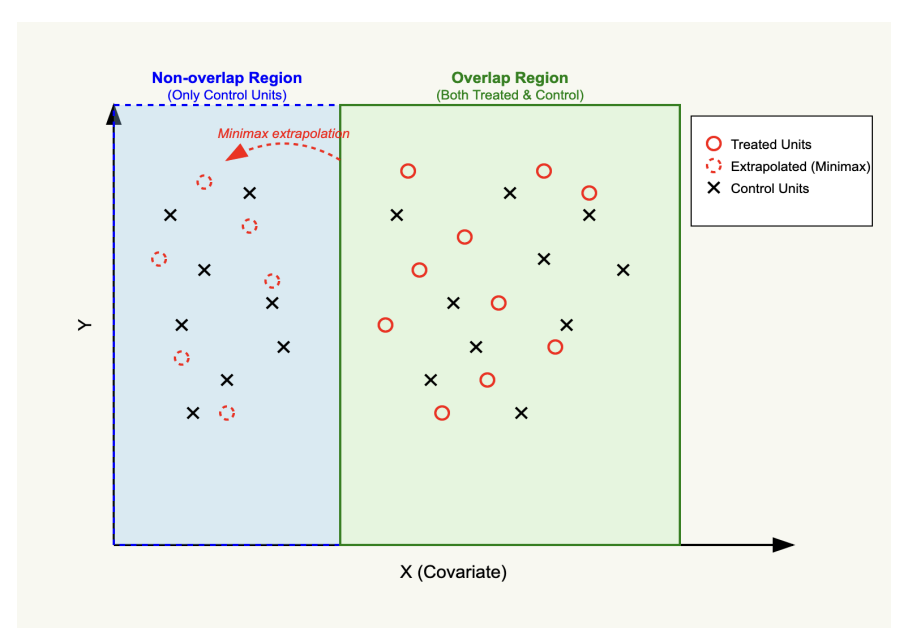


Figure 3. Visualization of our method. In the overlap region, we use typical asymptotic confidence intervals. In the non-overlap region, we use the minimax approach to extrapolate from the overlap region. Our method allows the analyst to analyze the potential bias caused by ignoring samples with extreme propensity scores and see how this depends on the extrapolability of data from the non-overlap region to the overlap region.

versions of asymptotic methods.

We begin by reviewing Donoho [14]'s minimax inferential framework in Section 2, then introduce our sensitivity analysis approach in Section 3. We provide some analytical insights in Section 2.3 and demonstrate our framework using both simulated and real datasets in Section 4. Our results illustrate how our sensitivity framework provides a simple diagnostic against asymptotic methods that silently fail. When compared to the naive minimax method [4], our approach yields significantly shorter intervals with comparable coverage properties. Finally, to inspire future work, we discuss potential extensions of our framework to adaptive data collection settings in Section 5.

Related work There is a substantial body of work studying observational analysis under limited overlap. These methods aim to rigorously characterize the statistical uncertainty associated with estimators such as IPW, AIPW, and matching-based methods, often under relaxed or irregular identification conditions. Khan and Tamer [32] and Rothe [46] show that in the presence of limited or vanishing overlap, the rate at which estimators converge to their true values can be significantly slower than the parametric \sqrt{n} rate, complicating standard inference. Yang and Ding [52] and Heiler and Kazak [19] extend this line of work by proposing robust inferential procedures that adjust for the heavy tails and large variances caused by extreme weights, which are especially problematic in regions of limited overlap.

Similarly, Hong et al. [20] and Ma and Wang [40] highlight how lack of overlap can lead to non-Gaussian asymptotic distributions, and they develop corrected inference procedures that better account for these irregularities. For instance, Ma and Wang [40] explicitly demonstrate the failure of conventional confidence intervals when the IPW estimator's asymptotic distribution departs from normality due to limited overlap. More recently, using a bias correction approach, Ma et al. [41]

propose doubly robust estimators that achieve valid asymptotic inference under weaker conditions, including near-zero overlap and high-dimensional covariates. On the other hand, our framework requires domain knowledge on the data-generating function (i.e., specifying the function class \mathcal{F} in a parametric form), but it provides non-asymptotic guarantees grounded in the minimax estimation literature, allowing for near-optimal finite-sample inference with explicit control over bias and variance trade-offs within a structured function class. This approach enables reliable inference even in challenging regions of the covariate space, without resorting to overly conservative bounds.

Another related line of work by Khan et al. [33] addresses the challenge of extrapolating treatment effects from the region of covariate overlap to the non-overlap region. Their method, which provides a point estimate of the treatment effect, builds on the partial identification literature [42, 25, 50, 12, 29], aiming to conservatively bound treatment effects in the non-overlap region. However, their approach depends critically on the accuracy of the fitted outcome model $\hat{\mu}$ in the overlap region, which is then extrapolated to the non-overlap region. This reliance means their guarantees can degrade when model fit is imperfect, especially in finite samples.

Our framework is closely related to the literature on minimax estimators, particularly the foundational work by Donoho [14] that introduces affine estimators that achieve near-optimal worst-case performance over specified function classes. Building on this, Armstrong and Kolesár [3, 4] apply the minimax approach to causal estimands, particularly without assuming strong overlap. Their approach yields estimators and confidence intervals with optimal worst-case performance, even when standard overlap assumptions fail. However, a key limitation of these methods is that the corresponding confidence intervals tend to be overly conservative, particularly in finite samples, due to their focus on worst-case performance across broad function classes.

In contrast, our method maintains the spirit of minimax optimality, but is more directly aimed at practical inference in regions of non-overlap, where conventional estimators perform poorly. As we detail in Section 2, our framework avoids the excess conservativeness of prior minimax-based intervals by applying the minimax approach only to analyze the non-overlap region.

2 Finite-sample minimax inference on regions of non-overlap

In this work, we assume that the observed units comprise the entire population of interest. This perspective is well-established in the causal inference literature [24, 2], and implies that the sample size n is fixed rather than drawn from a superpopulation. This modeling choice is particularly reasonable in many applied policy and healthcare settings, where the goal is to estimate causal effects for a specific, finite group—such as all patients in a registry, participants in a program, or residents of a region. In these scenarios, inference does not concern some hypothetical infinite population, but rather the actual individuals in the dataset. By treating the population as fixed, we avoid assumptions about the data-generating process beyond what is necessary for causal identification, and we can directly quantify uncertainty due to lack of overlap or sparsity in observed units. This approach also aligns well with our focus on evaluating uncertainty in finite samples and identifying regions with poor support, where asymptotic approximations may fail. We would also like to point out that though many estimators in the literature focus on the population-level treatment effects, they can be used to estimate the sample average treatment effect [24].

Formally, we consider the standard potential outcome framework where the observed tuples $\{x_i, y_i, z_i\}_{i=1}^n$ consist of treatment $z_i \in \{0, 1\}$ alongside covariates x_i . Our goal is to estimate the

sample average treatment effect (ATE)

$$\tau := \frac{1}{n} \sum_{i=1}^{n} \mathbb{E}[Y_i(1) - Y_i(0) | X_i = x_i]. \tag{2.1}$$

under the assumption of unconfoundedness $(Y_i(1), Y_i(0)) \perp Z_i \mid X_i$. This is also sometimes called conditional average treatment effect [24, 2]. More generally, for known weights $w_i \geq 0$, we are interested in the weighted average treatment effect

$$\tau_{\mathbf{w}}(f) := \sum_{i=1}^{n} w_i \tau(f, x_i) \text{ where } \tau(f, x) := f(x, 1) - f(x, 0).$$
 (2.2)

Since f is unknown, we omit its explicit dependence in $\tau_{\boldsymbol{w}}(f)$ and $\tau(f, x_i)$.

To obtain reliable estimates of the ATE, the strong overlap assumption [45, 24] states that the propensity score $\pi(x) := \mathbb{P}(z=1|x=x)$ is bounded away from 0 and 1:

$$\varepsilon < \pi(x_i) < 1 - \varepsilon$$
 for some $\varepsilon > 0$ for all i.

When facing limited overlap, researchers truncate/winsorize the fitted propensity score at some level that makes the resulting estimator stable. This implicitly changes the estimand to units with sufficient overlap. As we observed in Example 1, without truncation, the confidence intervals typically blow up. On the other hand, as we show in Section D.1, truncation could lead to substantial undercoverage under limited overlap.

Throughout, we assume the propensity score $\pi(x)$ is known and show that standard asymptotic estimators can still fail under this idealized setting, highlighting the inherent challenges posed by limited overlap. As we will see, our framework requires minimal knowledge of the propensity score and thus can be easily generalized to the setting with unknown propensity scores. In addition, for most parts of the paper, we assume the analyst follows a particular trimming procedure that divides the data into non-overlap and overlap regions.

2.1 Background

Before we introduce our approach, we first provide background on an inferential framework built on the theory of minimax estimation for linear functions [14, 7, 4]. Instead of relying on central limit theorems that assume an infinite stream of data generated by a fixed data-generating distribution, this framework generates a worst-case confidence interval over all data-generating distributions that could have generated the sample the researcher has access to.

We assume there is an unknown data-generating function f with

$$y_i = f(x_i, z_i) + \epsilon_i,$$

where $\epsilon_i \sim N(0, \sigma^2(x_i, z_i))$ is the independent Gaussian noise with known variance. Since we are not in the asymptotic regime, we impose an explicit distributional assumption on the noise. This framework can be generalized to other distributional assumptions as discussed in Juditsky and Nemirovski [27]. As discussed in Section 4, we can estimate σ from data and the framework remains applicable.

The unknown function f is assumed to be within a known function class \mathcal{F} , which is prespecified and reflects the researcher's prior knowledge on all possible functions that could have generated the observed data. We focus on generating confidence intervals \mathcal{C} with guaranteed coverage of the

desired estimand $\tau_{\boldsymbol{w}}(f)$ when the true generating function satisfies $f \in \mathcal{F}$:

$$\inf_{f \in \mathcal{F}} \mathbb{P}_f(\tau_{\boldsymbol{w}}(f) \in \mathcal{C}) \ge 1 - \alpha. \tag{2.3}$$

We usually assume α is a fixed quantity, e.g., $\alpha = 0.05$. Recalling that we assume the population and sample size n are fixed, we omit the dependence of the estimand on n in the paper. We focus on centrosymmetric sets $(f \in \mathcal{F} \text{ implies } -f \in \mathcal{F})$ as it simplifies the expression of the minimax estimator to be introduced (see, e.g. [4]).

After fixing the function class \mathcal{F} and data \mathcal{D} , the minimax confidence interval of $\tau_{\boldsymbol{w}}$ (2.2) is governed by the following quantity that is known as the *modulus of continuity* [14]:

$$\omega_{\mathcal{F};\mathcal{D}}(\delta; \boldsymbol{w}) := \sup_{f \in \mathcal{F}} \left\{ \sum_{i=1}^{n} 2w_i \left(f(x_i, 1) - f(x_i, 0) \right) : \sum_{i=1}^{n} \frac{f^2(x_i, z_i)}{\sigma^2(x_i, z_i)} \le \frac{\delta^2}{4} \right\}. \tag{2.4}$$

The parameter δ controls the weights as we visualize through an example in the next subsection. We discuss how to compute $\omega_{\mathcal{F};\mathcal{D}}$ in Appendix B.

Letting the optimal solution of (2.4) be $f_{\delta}^{\star}(x_i, z_i)$, one then computes $\omega(\delta; \boldsymbol{w})$ for every $\delta > 0$, and each δ yields a corresponding minimax estimator [3, 4] $\hat{\tau}_{\delta}(\boldsymbol{w})$ given by

$$\hat{\tau}_{\delta}(\boldsymbol{w}) = \sum_{i=1}^{n} \frac{2\omega'(\delta)}{\delta} \frac{f_{\delta}^{\star}(x_i, z_i)}{\sigma^2(x_i, z_i)} y_i = \left(\sum_{i=1}^{n} w_i\right) \sum_{i=1}^{n} \frac{f_{\delta}^{\star}(x_i, z_i)/\sigma^2(x_i, z_i)}{\sum_{j=1}^{n} z_j f_{\delta}^{\star}(x_j, z_j)/\sigma^2(x_j, z_j)} y_i, \tag{2.5}$$

where f^* is an optimal solution of (2.4). In addition,

$$C_{\delta}(\boldsymbol{w}) = \hat{\tau}_{\delta}(\boldsymbol{w}) \pm \operatorname{cv}_{\alpha} \left(\frac{\overline{\operatorname{bias}}(\hat{\tau}_{\delta}(\boldsymbol{w}))}{\operatorname{sd}(\hat{\tau}_{\delta}(\boldsymbol{w}))} \right) \operatorname{sd}(\hat{\tau}_{\delta}(\boldsymbol{w}))$$
(2.6)

is a valid confidence interval that applies a bias correction procedure on top of $\hat{\tau}_{\delta}(\boldsymbol{w})$, where $\operatorname{cv}_{\alpha}(b)$ is the $1-\alpha$ quantile of a |N(b,1)| random variable. In (2.6),

$$\overline{\operatorname{bias}}(\hat{\tau}_{\delta}(\boldsymbol{w})) := \sup_{f \in \mathcal{F}} \mathbb{E}_{f} \Big[\hat{\tau}_{\delta}(\boldsymbol{w}) - \tau_{\boldsymbol{w}}(f) \Big]$$
(2.7)

is the maximum possible bias of $\hat{\tau}_{\delta}(\boldsymbol{w})$, which can be shown [4] to be equal to

$$\overline{\text{bias}}(\hat{\tau}_{\delta}(\boldsymbol{w})) = \frac{1}{2}(\omega(\delta; \boldsymbol{w}) - \delta\omega'(\delta; \boldsymbol{w})). \tag{2.8}$$

In addition, the standard error of the estimator can be computed by

$$sd(\hat{\tau}_{\delta}(\boldsymbol{w})) = \omega'(\delta; \boldsymbol{w}). \tag{2.9}$$

After obtaining (2.6) for every δ , we construct the minimax CI using δ_{FLCI} , where δ_{FLCI} is chosen by solving the following problem to minimize the CI length balancing bias and variance of $\hat{\tau}_{\delta}(\boldsymbol{w})$:

$$\delta_{\text{FLCI}}(\boldsymbol{w}) \in \underset{\delta>0}{\operatorname{argmin}} \left\{ \operatorname{cv}_{\alpha} \left(\frac{\overline{\operatorname{bias}}(\hat{\tau}_{\delta}(\boldsymbol{w}))}{\operatorname{sd}(\hat{\tau}_{\delta}(\boldsymbol{w}))} \right) \operatorname{sd}(\hat{\tau}_{\delta}(\boldsymbol{w})) \right\}, \tag{2.10}$$

which yields the minimax CI, denoted as $\mathcal{C}_{\delta_{\mathrm{FLCI}}}(\boldsymbol{w})$. This construction determines the shortest possible length for fixed-length confidence procedures under a given function class, and the associated modulus-based confidence interval attains this minimax criterion. Importantly, the optimal

modulus procedure admits an implementation that is affine in the outcomes (an affine estimator together with a calibrated bias correction). As Armstrong and Kolesár [4, Theorem A.3] show, this confidence interval is minimax-optimal among all fixed-length procedures.

In this work, we follow Armstrong and Kolesár [4] and focus on Lipschitz outcome functions

$$\mathcal{F}_{L,\|\cdot\|} := \{ f : |f(x,d) - f(\tilde{x},d)| \le L \|x - \tilde{x}\|, \forall x, \tilde{x} \in \mathcal{X}, d \in \{0,1\} \}.$$
 (2.11)

It is well known that we can replace the constraint \mathcal{F} with its finite-sample counterpart and only impose Lipschitz constraints on the observed n data points [5], which we denote as

$$\mathcal{F}_{L,\|\cdot\|,n} := \{ f : |f(x_i,d) - f(x_j,d)| \le L \|x_i - x_j\|, \forall i, j \in [n], d \in \{0,1\} \}.$$
 (2.12)

Henceforth, we focus on the ℓ_2 norm and use \mathcal{F}_L to represent $\mathcal{F}_{L,\ell_2,n}$.

2.2 Proposed approach

Applying the finite-sample minimax approach over the entire dataset [4] can be pessimistic, as it focuses on the worst-case function within a given function class. For the Lipschitz function class, Theorem 2.3 of Armstrong and Kolesár [4] demonstrates that the minimax estimator relies only on information from nearby points—especially when the Lipschitz constant L is large—for counterfactual imputation. This occurs even when distant points, whose outcomes are observed and potentially informative, are available. As a result, the minimax method may fail to fully utilize all available information, leading to practically inefficient inference, as we demonstrate in the next section. Another notable feature of the minimax approach is that the resulting confidence interval length does not depend on the observed outcomes y_1, \ldots, y_n . This further highlights its conservative nature, particularly in regions where outcome data alone are insufficient to justify narrower intervals.

This conservatism is well-suited for analyzing regions of *non-overlap*, where no comparable treated or control units are observed and traditional estimation methods become unreliable. In such settings, the inherently cautious nature of minimax inference provides an honest reflection of the uncertainty stemming from a lack of overlap.

We thus study minimax confidence intervals $C_{\delta_{\text{FLCI}}}(\boldsymbol{w})$ on regions of non-overlap (abbreviated as $M_{\boldsymbol{w}}$). Intuitively, $M_{\boldsymbol{w}}$ can be used to bound the bias of any estimator targeting

$$\tau_{\bar{w}} := \sum_{i=1}^{n} \left(\frac{1}{n} - w_i\right) \tau(x_i),$$

i.e., the complement of $\tau_{\boldsymbol{w}}$ relative to the full-sample ATE. In addition to reweighted estimands proposed by Crump et al. [10], the family of estimators $\hat{\tau}_{\boldsymbol{w}}$ includes standard truncated estimators such as AIPW_{partial} as discussed before. By ignoring regions with poor overlap, these estimators aim to estimate $\tau_{\bar{\boldsymbol{w}}}$ —the ATE over the region with overlap—with greater accuracy, at the cost of potentially larger bias $\tau_{\bar{\boldsymbol{w}}} - \tau$ even when these estimators are unbiased. Our framework, $M_{\boldsymbol{w}}$, provides a principled framework to analyze this bias.

Though our framework is general, we focus on using it as an auxiliary tool for typical asymptotic estimators such as $\mathsf{AIPW}_{\mathsf{partial}}$. Our proposed method, minimax partial (MP_{ϵ}) , is parameterized by the truncation threshold $\epsilon \in (0, \frac{1}{2})$ on the propensity score chosen by the practitioner when they truncate the data in $\mathsf{AIPW}_{\mathsf{partial}}$, and only applies the minimax approach on the non-overlap region. Throughout, we define

$$q(x) = \min \{ \pi(x), 1 - \pi(x) \}$$
 (2.13)

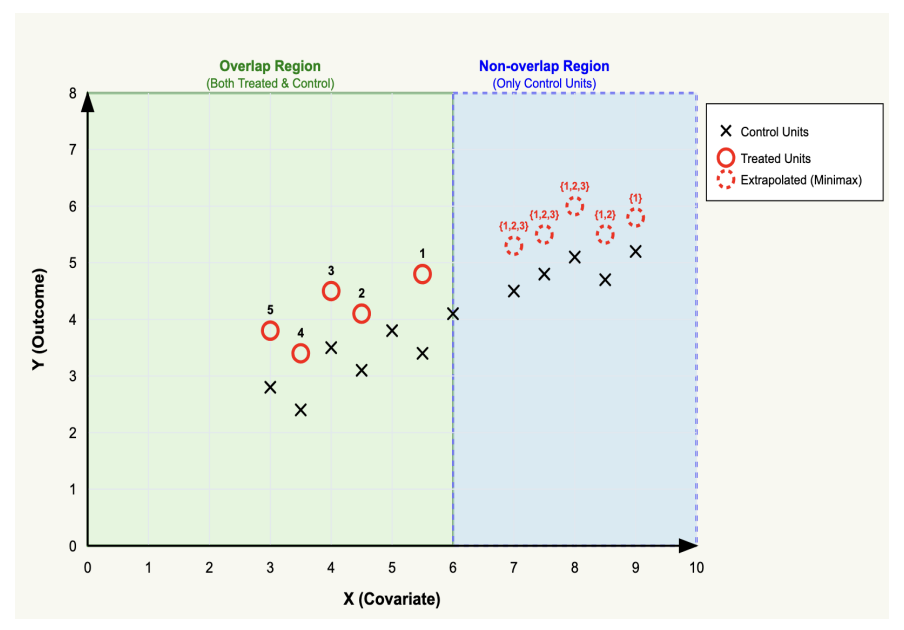


Figure 4. For each point in the non-overlap region, we list the set of treated points from the overlap region used in its extrapolation. For example, the leftmost point i in the non-overlap region uses points 1, 2, and 3 for extrapolation. This means that point pairs (i,1),(i,2),(i,3) have binding Lipschitz constraints for the program that defines the minimax estimator $\hat{\tau}_{\delta_{\text{FLCI}}}(\boldsymbol{w})$ (2.5).

as a measure of overlap for each point x. Given a fixed ϵ , we decompose the ATE τ as follows:

$$\tau = \mathbb{P}(q(X) \ge \epsilon) \mathbb{E}[\tau(X)|q(X) \ge \epsilon] + \mathbb{P}(q(X) < \epsilon) \mathbb{E}[\tau(X)|q(X) < \epsilon] := \tau_+ + \tau_-, \tag{2.14}$$

where we assume $X \sim \widehat{P}_n$, the empirical distribution formed by data $\{x_i\}_{i \in [n]}$. Based on the above expression, we define MP_ϵ as

$$\mathsf{MP}_{\epsilon} := \mathsf{M}_{\boldsymbol{w}_{\epsilon}},\tag{2.15}$$

where $(\boldsymbol{w}_{\epsilon})_i = \frac{1}{n} \mathcal{I} (q(x_i) < \epsilon)$.

Sometimes we also write $\mathsf{MP}_{\epsilon,L}$ to emphasize that we assume the function class is \mathcal{F}_L (2.11). We omit the dependence on ϵ and simply write MP when the dataset is fixed, assuming that the truncation threshold ϵ is selected using a standard procedure. Using the interval MP_{ϵ} , we can construct a metric to evaluate the underlying uncertainty in the non-overlap region. For example, letting $[\mathsf{MP}_{\epsilon}^-, \mathsf{MP}_{\epsilon}^+]$ be the interval MP_{ϵ} , we consider the following metric as a way to estimate τ_-

$$T(\mathsf{MP}_{\epsilon}) := \max\left\{ |\mathsf{MP}_{\epsilon}^{-}|, |\mathsf{MP}_{\epsilon}^{+}| \right\}, \tag{2.16}$$

which is the largest absolute value of the interval end points generated by MP_{ϵ} . The larger this value is, the more bias $\mathsf{AIPW}_{\mathsf{partial}}$ can lead to. Similarly, we can use $T(\mathsf{MP}_{\epsilon}) = |\mathsf{MP}_{\epsilon}|$ to estimate the uncertainty of the bias estimate.

2.3 Analytic insights

Since the derivation of the minimax estimator is involved, we provide some analytical intuition.

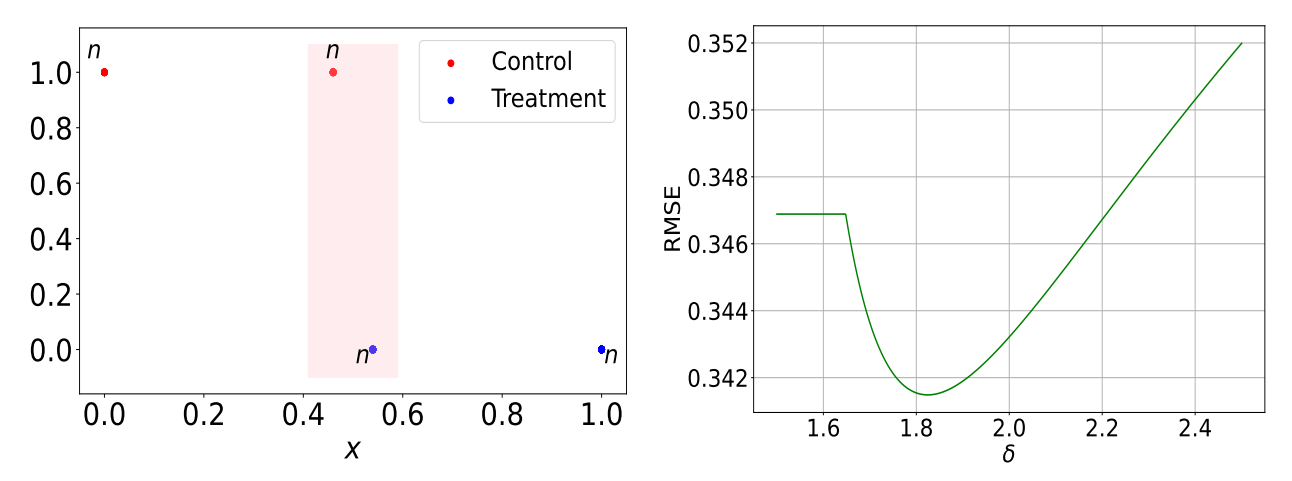


Figure 5. Left: There are 2(k+1)n samples in total and the middle region in pink is the overlap region. See Appendix C for details. **Right**: RMSE of the estimator $\hat{\tau}_{\delta}(\boldsymbol{w})$ vs δ with $n=25, k=10, L=1, \eta=0.1, \xi=0.01$.

Matching interpretation We start by interpreting the minimax estimator as a nearest-neighbor estimator.

Lemma 1. Let $\mu \geq 0$ and $\Lambda \geq 0$ be the optimal dual variables corresponding to the Lipschitz constraints (2.12). The minimax estimator imputes counterfactual values as

$$w_k \hat{f}(x_k, 1 - z_k) = \sum_{j: z_j = 1 - z_k} W_{jk} y_j \quad \text{where} \quad W_{jk} = \begin{cases} \frac{\Lambda_{jk}^1}{\mu}, & \text{if } z_k = 0\\ \frac{\Lambda_{kj}^0}{\mu}, & \text{if } z_k = 1. \end{cases}$$
(2.17)

See Appendix A for the proof.

To illustrate, consider a simple dataset where the data is divided into overlap and non-overlap regions; in the non-overlap region, no samples receive treatment and the minimax estimator relies on the treatment data from the overlap region to perform extrapolation. Figure 4 shows how extrapolation is being conducted by MP: matching weights W_{jk} (A.4) are computed only using (X, Z) data and nonzero only if the corresponding Lipschitz constraints (2.12) for point (j, k) are binding.

Extrapolation in regions of non-overlap In particular, consider a one-dimensional setting with two clusters of covariates $x \in \mathbb{R}$ (n points in total): one with positive weights and the other without. That is, there exists $t \in \mathbb{R}$ such that for all $x_i \leq t$, we have $w_i = 0$ and for all $x_i > t$, we have $w_i = \frac{1}{n}$. We can prove that our minimax procedure respects the geometry of the covariate space when extrapolating: if it chooses to extrapolate using a unit j farther from the non-overlap region, then it must also be using all closer points. Recall the modulus of continuity on the non-overlap region (assuming $\sigma^2 = 1$ for simplicity)

$$\omega(\delta) = \max_{f \in \mathcal{F}_L} 2 \sum_{i=1}^n w_i (f(x_i, 1) - f(x_i, 0))$$

$$\text{s.t.} \quad \sum_{i=1}^n f(x_i, z_i)^2 \le \frac{\delta^2}{4},$$
where $w_i = \frac{1}{n} \mathcal{I}(q_i < \epsilon)$ (2.18)

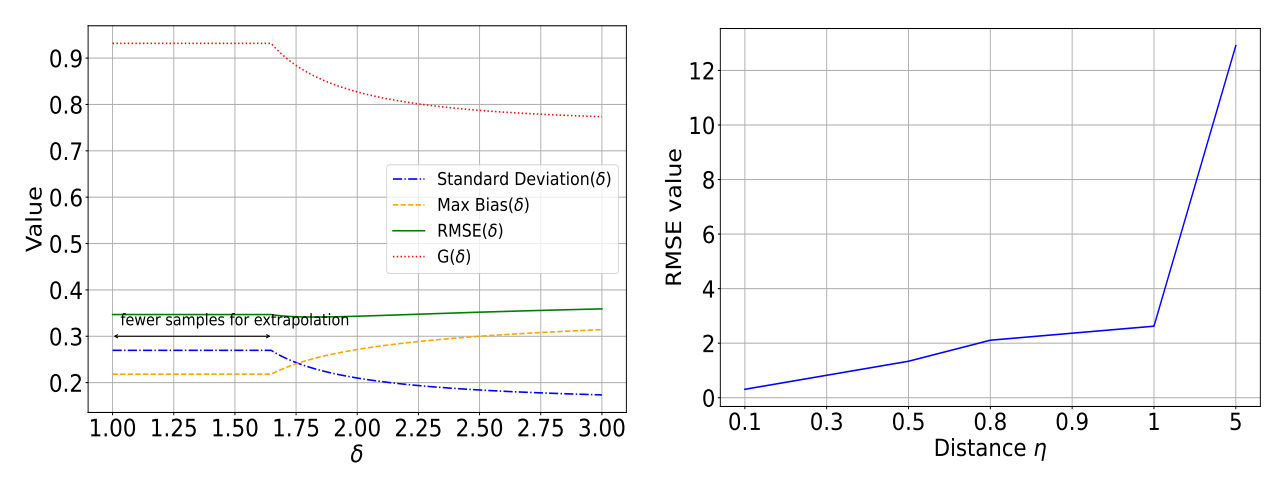


Figure 6. Left: Bias, variance, and the length of the confidence interval (2.6) $G(\delta) = \operatorname{cv}_{\alpha}\left(\frac{\overline{\operatorname{bias}}(\hat{\tau}_{\delta}(\boldsymbol{w}))}{\operatorname{sd}(\hat{\tau}_{\delta}(\boldsymbol{w}))}\right) \cdot \operatorname{sd}(\hat{\tau}_{\delta}(\boldsymbol{w}))$. Right: RMSE as we vary the distance parameter η ; for each η , we compute the optimal (lowest) RMSE with respect to $\delta \geq 0$.

and for all i with $w_i = 0$, let $\eta_i = \min_j \{|x_i - x_j| \mid w_j > 0\}$ denote its distance to the region with positive weights. The following result shows that extrapolation starts from the boundary of the overlap region and proceeds inward.

Lemma 2. Consider two units i and j with $w_i = w_j = 0$ and $\eta_i \ge \eta_j$. Then for every $\delta > 0$, there exists an optimal solution f_{δ}^{\star} to the optimization problem (2.18) with $f_{\delta}^{\star}(x_j, 1) \ge f_{\delta}^{\star}(x_i, 1)$.

Estimation error as a function of δ Finally, we shed light on the bias (2.8) and variance (2.9) of our minimax approach as a function of δ (2.4), which controls the total weight the estimator is allowed to place. On the left panel of Figure 5, we consider 2n samples with treatment assignments z = 1 and z = 0 located within the *overlap region* (with distance ξ), and an additional $2k \cdot n, k > 1$ samples located at a distance η outside of this region (i.e., without overlap). This structure allows us to compute the modulus of continuity $\omega(\delta)$ in closed form for all $\delta > 0$, which we then use to analyze the worst-case bias and variance.

To understand the bias-variance trade-off more closely, in the left panel of Figure 6, we plot the worst-case bias $\overline{\text{bias}}(\hat{\tau}_{\delta}(\boldsymbol{w}))$ and the standard deviation $\mathrm{sd}(\hat{\tau}_{\delta}(\boldsymbol{w}))$ separately.

- When δ is *small*, the estimator uses fewer samples for extrapolation, so it has lower bias and higher variance.
- When δ is *large*, the estimator uses more samples for extrapolation, reducing variance at the cost of increased bias.

In the right panel of Figure 6, we further explore how the optimal RMSE obtained by optimizing over δ scales with the lack of overlap η . As η increases, extrapolation becomes less reliable, leading to higher RMSE.

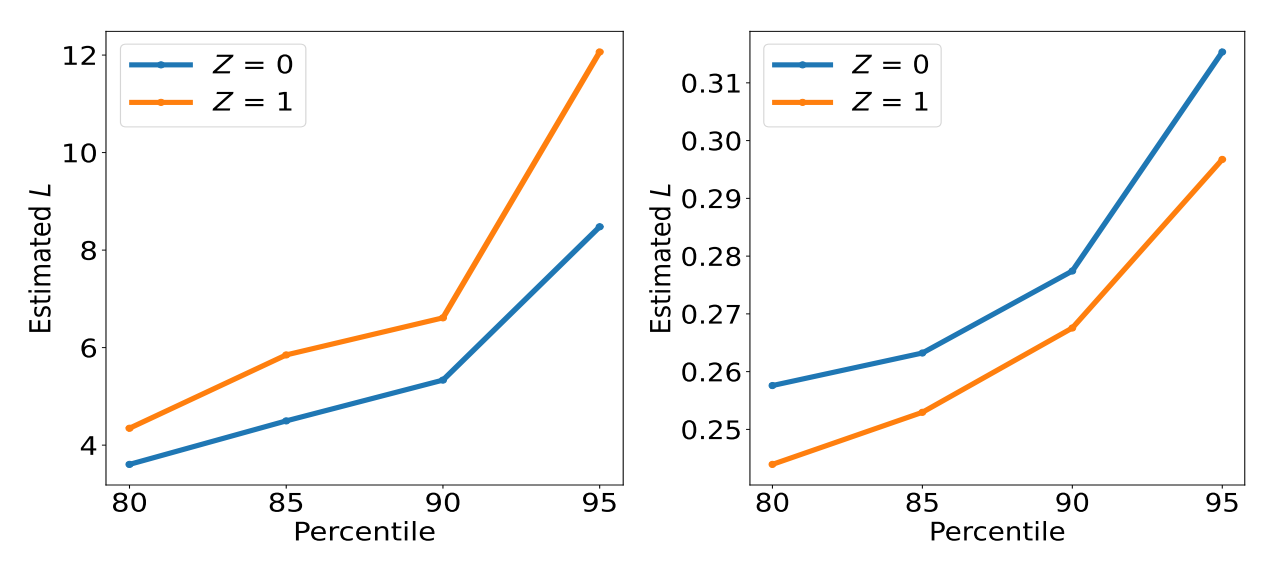


Figure 7. Contextualization of the Lipschitz constant $\tilde{L}_{Z,p}$ (3.1) vs p. Left: Example 1. Right: PennUI dataset in Section 4

3 Sensitivity analysis

We use the MP framework to facilitate a diagnostic analysis assessing how different levels of assumed smoothness affect the estimate of bias due to trimming. Our framework asks how strong the extrapolation assumption must be for the induced bias of the asymptotic estimator to remain negligible? Instead of committing to a level of L—which is inherently challenging—our sensitivity framework varies the Lipschitz constant L to assess how the minimax interval $\mathsf{MP}_{\epsilon,L}$ evolves in length and location. This allows analyzing the relationship between the assumed smoothness of the outcome function and the potential bias due to trimming. Small values of L correspond to strong smoothness assumptions—implying high extrapolability, while larger values represent weaker assumptions and lead to wider, more conservative intervals.

To contextualize the sensitivity curve, we use the overlap region (where we trust the predicted outcome regressor) to estimate the smoothness of the outcome function, and use this estimate to guide how to properly model the outcome function in the non-overlap region. A uniform Lipschitz constant over all data points (i.e., taking the maximum instead of the quantile in (3.1)) may be overly conservative due to data noise. We consider the p-th quantile of $\frac{\hat{\mu}_Z(x_i) - \hat{\mu}_Z(x_j)}{\|x_i - x_j\|}$ (where $\hat{\mu}$ is the fitted outcome regressor using data in the overlap region)

$$\tilde{L}_{Z,p} = \max_{i:q(x_i) \ge \epsilon} \left\{ p - \text{th quantile } \left\{ j \ne i, q(x_j) \ge \epsilon : \left| \frac{\hat{\mu}_Z(x_i) - \hat{\mu}_Z(x_j)}{\|x_i - x_j\|} \right| \right\} \right\}, Z \in \{0, 1\}.$$
 (3.1)

Since contextualizing the Lipschitz constant L is challenging, the analyst can instead think of the more intuitive quantity $p \in (0,1)$ that controls the functional class. For simplicity, we consider the uniform Lipschitz constant estimate for $Z \in \{0,1\}$ and consider

$$\tilde{L}_p = \max_{Z \in \{0,1\}} \left\{ \tilde{L}_{Z,p} \right\}. \tag{3.2}$$

Using L_p in our framework, the analyst can better articulate the function spaces parameterized by L. In addition, the choice of p to make the confidence intervals valid also forms useful domain

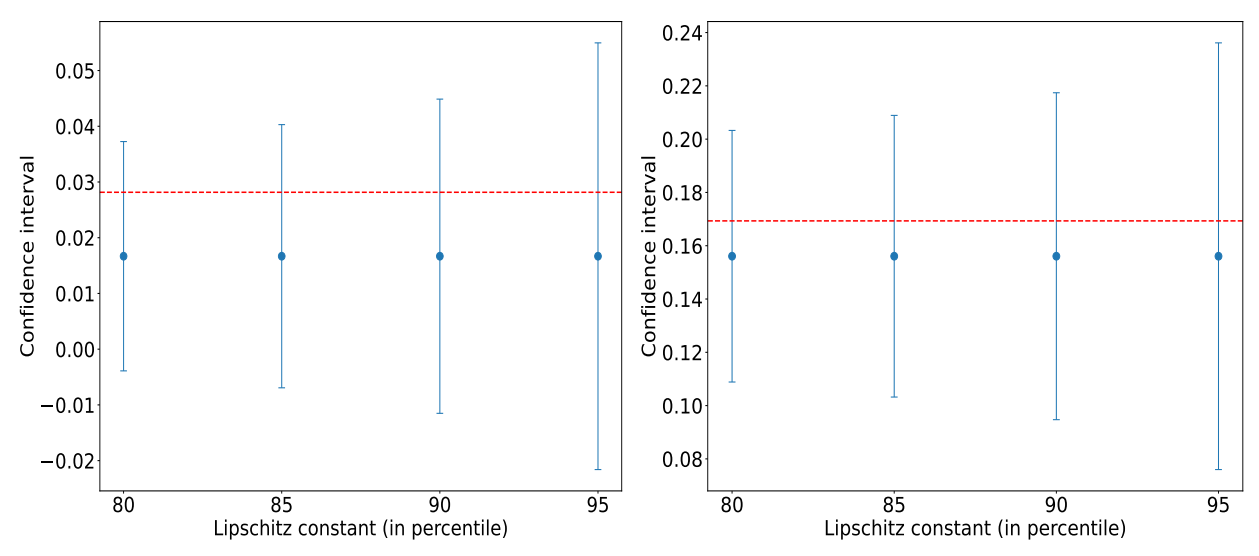


Figure 8. Data comes from Example 1. On the left, we have confidence intervals generated by MP_{ϵ} at different values of L with $\epsilon=0.01$. We see how increasing the value of L covers the estimand τ_{-} and this enables the sensitivity analysis. On the right, we have results for M. As we can see, the confidence intervals M are much wider than MP.

knowledge and can be potentially transferred to other datasets. In Figure 7, we use Example 1 to numerically illustrate this contextualization approach. We observe that the percentile-based contextualization procedure offers an interpretable and data-driven way to vary the extrapolation assumptions and examine their impact on inference.

Illustrating our sensitivity framework using Example 1 Figure 8 shows $MP_{\epsilon,L}$ across Lipschitz constants L for a fixed $\epsilon = 0.01$, which is the threshold that minimizes the length of the confidence interval AlPW_{partial} as in (1.2); we consider L ranging from \hat{L}_p (3.2) with p = 0.80 to p = 0.95, which roughly corresponds to L ranging from L = 5 to L = 14 from Figure 7.

Our analysis shows how gradually increasing L—and thus weakening the smoothness assumption-leads to wider confidence intervals from $\mathsf{MP}_{\epsilon,L}$, but also improves coverage of the ATE in the non-overlap region τ_- . This trend reflects that under stronger smoothness assumptions (lower L), the minimax procedure may underestimate uncertainty, whereas more conservative values of L yield intervals that reliably contain τ_- . The sensitivity framework clearly allows the analyst to better understand the assumptions. For example, at the 80th percentile, we see the MP_{ϵ} interval is almost entirely above 0, suggesting a larger chance of having a positive bias. For a larger percentile, or being more conservative, we see MP becomes much wider, and the potential magnitude of the bias also increases. Concretely, in Figure 9 we summarize our minimax partial estimator MP at the 95th percentile L (L=14) where we observe reliable coverage while maintaining reasonably short confidence intervals.

Combining confidence intervals If the analyst deems the asymptotic approach to be untrust-worthy, they can either modify the estimand so that excluding the uncertain subpopulation is acceptable, or adopt a hybrid confidence interval that employs a conservative union bound to combine the intervals from the minimax and asymptotic approaches. Specifically, in Figure 9, when the non-overlap parameter is 0.03, the length of MP is even wider than AlPW_{partial} and the analyst

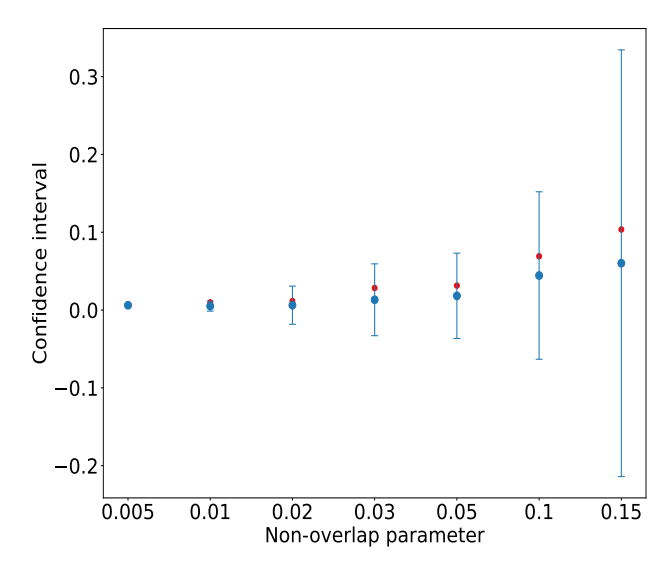


Figure 9. We plot MP_ϵ with a fixed Lipschitz constant L=14 with different values of non-overlap parameter η . In this plot, red points represent the non-overlap ATE at each value of the non-overlap parameter. Blue points/intervals represent the point estimate/confidence interval of MP. At every point, we assume the truncation threshold is chosen to minimize the length of the AIPW partial interval. This shows the MP interval adapts to data with different levels of overlap.

can consider improving coverage while mitigating the excessive length often associated with purely minimax-based intervals. Using the union bound $\mathbb{P}(X+Y\geq x+y)\leq \mathbb{P}(X\geq x)+\mathbb{P}(Y\geq y)$, we can add the upper bounds of AIPW_{partial} and MP at levels $\alpha/2$ (i.e., coverage with probability $1-\alpha/2$) to obtain an α -confidence interval of MP_{combine}: the combined α -confidence interval of τ is

$$\mathsf{MP}_{\mathsf{combine}}^{(\alpha)} = \left[a_1 + b_1, a_2 + b_2 \right], \quad \text{where} \quad \mathsf{AIPW}_{\mathsf{partial}}^{(\alpha/2)} = \left[a_1, a_2 \right], \quad \mathsf{MP}^{(\alpha/2)} = \left[b_1, b_2 \right]. \tag{3.3}$$

Coverage probability To assess the coverage probability of different inferential approaches, we evaluate the performance of different confidence interval procedures across repeated trials in Figure 10. We observe a sharp decline in the coverage probability for AIPW_{partial} as η increases from 0.005 to 0.03. This highlights the fragility of asymptotic methods under violation of the overlap assumption and underscores the utility of our framework in providing reliable inference where standard estimators fail.

Despite achieving the desired coverage, the full minimax procedure M is overly conservative: its length is significantly larger than necessary and does not meaningfully reflect the uncertainty specifically attributable to the non-overlap region. In contrast, the interval from MP, which targets τ_{-} , is substantially narrower and better calibrated to the uncertainty in the trimmed region. The combined interval MP_{combine} achieves valid coverage for the full ATE τ , with a shorter length (higher power) than the conservative interval from M for small values of η .

4 Case study

We now demonstrate our framework through a case study on the Pennsylvania Reemployment Bonus Demonstration (PennUI) dataset, a significant experiment conducted from 1988 to 1989 to

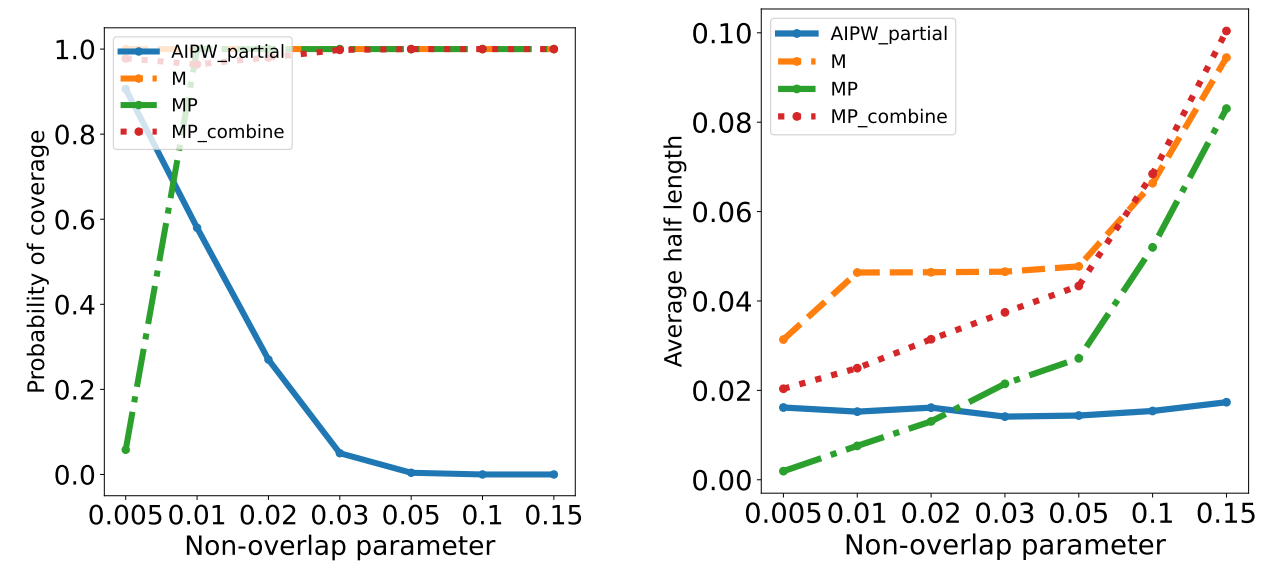


Figure 10. Probability of coverage and half length for L=14, as we vary the non-overlap parameter η (D.1). The truncation threshold is always chosen to be the one such that AIPW_{partial} has the smallest length. Our method MP helps analyze the unreliability of AIPW_{partial}.

estimate the impact of financial incentives on reemployment [34].

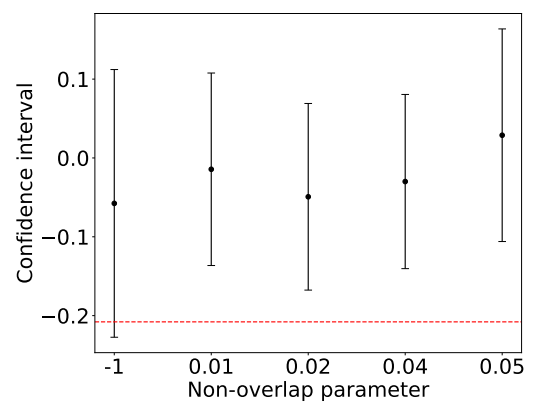
Preliminaries In the PennUI dataset, approximately 15,000 eligible claimants were randomly assigned to one of the six treatment groups or a control group. The data provides valuable insights for policymakers aiming to enhance reemployment programs and UI (unemployment insurance) systems. In this dataset, the outcome variable Y is the log of the duration of unemployment for the UI claimant and covariates $X \in \mathbb{R}^{60}$ include demographics and employment service program participation. We take a subset of this data, considering only treatment variable taking values in $\{4,6\}$ and further conduct a random subsampling with n=539 samples with roughly 48.3% of the samples received treatments. As this data is a randomized experiment, we can use a standard difference-in-means estimator to obtain the treatment effect $\tau=-0.2$ on the entire population.

We simulate various observational datasets using a sampling method with more details in Section D. To define the propensity score used in the sampling procedure, we first train a T-learner using Random Forest regressors on the entire dataset to obtain $\hat{\tau}(x_i)$ for all points x_i , then we map the value of $\hat{\tau}(x_i)$ to obtain $\pi_{\eta}(x_i) = E_{\eta}(\text{percentile}(\hat{\tau}(x_i)))$ for each sample i with

$$E_{\eta}(x) = \begin{cases} \operatorname{Uni}(0.005, 0.03) & \text{if } x \le 0.075 + \eta \text{ or } 1 - x \le 0.075 + \eta \\ \operatorname{Uni}(0.03, 0.05) & \text{elif } x \le 0.1 + \eta \text{ or } 1 - x \le 0.1 + \eta \\ \operatorname{Uni}(0.05, 0.1) & \text{elif } x \le 0.15 + \eta \\ 0.5 & \text{otherwise} \end{cases}$$
(4.1)

We assign extreme values of $\pi_{\eta}(x_i)$ to those with extreme values of $\hat{\tau}$ and it leads to observational datasets with limited overlap. Unless otherwise specified, we assume $\eta = 0.01$. Now, for AIPW or AIPW_{partial}, we use a Random Forest regressor for the outcome prediction.

Recall that the standard deviation σ is an important input to our procedure MP. To estimate



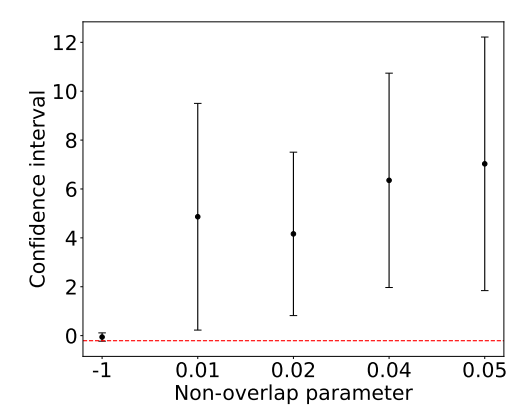


Figure 11. Failure of AIPW_{partial} on observational data simulated from the PennUI dataset. Similar to Figure 2, we compare the confidence interval from AIPW_{partial} for data generated with different levels of η in (4.1), and $E_{-1}(x) = \frac{1}{2}$ for all x. Left: With truncation. Right: Without truncation.

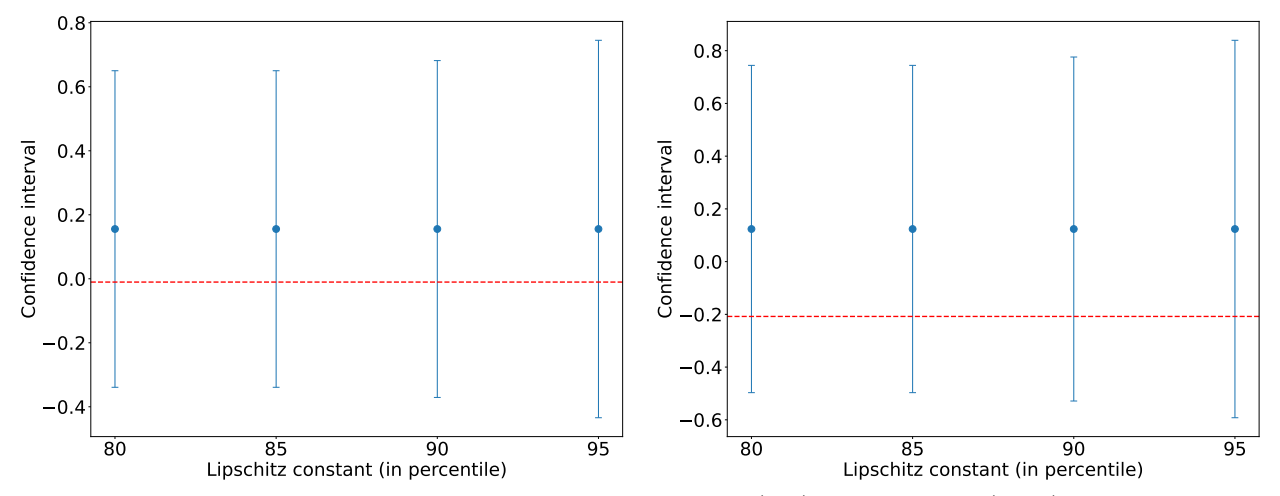


Figure 12. Real data results: confidence intervals for MP_{ϵ^*} (left) and $\mathsf{MP}_{\mathsf{combine}}$ (right) at different L for $\eta = 0.01$. The red dotted points are τ_- and τ respectively. The data is the same as in Figure 11.

it, we utilize the same estimator as in [1, 4], which is given by

$$\widehat{\sigma}^2 := \frac{1}{n} \sum_{i=1}^n \widehat{\sigma}^2(x_i, z_i) \quad \text{where} \quad \widehat{\sigma}^2(x_i, z_i) = \frac{J}{J+1} \left(Y_i - \frac{1}{J} \sum_{m=1}^J Y_{\ell_m(i)} \right)^2. \tag{4.2}$$

Here, $\ell_m(i)$ is the closest unit to unit i among the units with the same treatment as unit i and J is a tuning parameter which we choose to set as J=2 following [4].

Failure of asymptotic estimators In Figure 11, we observe that $AIPW_{partial}$ does not cover τ as the lack of overlap becomes more severe. The output of $AIPW_{partial}$ significantly overestimates the treatment effect, and we see the upper bound of the interval deviates significantly from the true treatment effect. (Similar to our running simulation example, we assume the analyst chooses the truncation threshold from the set $\mathcal{E} = \{0.01, 0.02, 0.03, 0.04, 0.05, 0.06, 0.07\}$.)

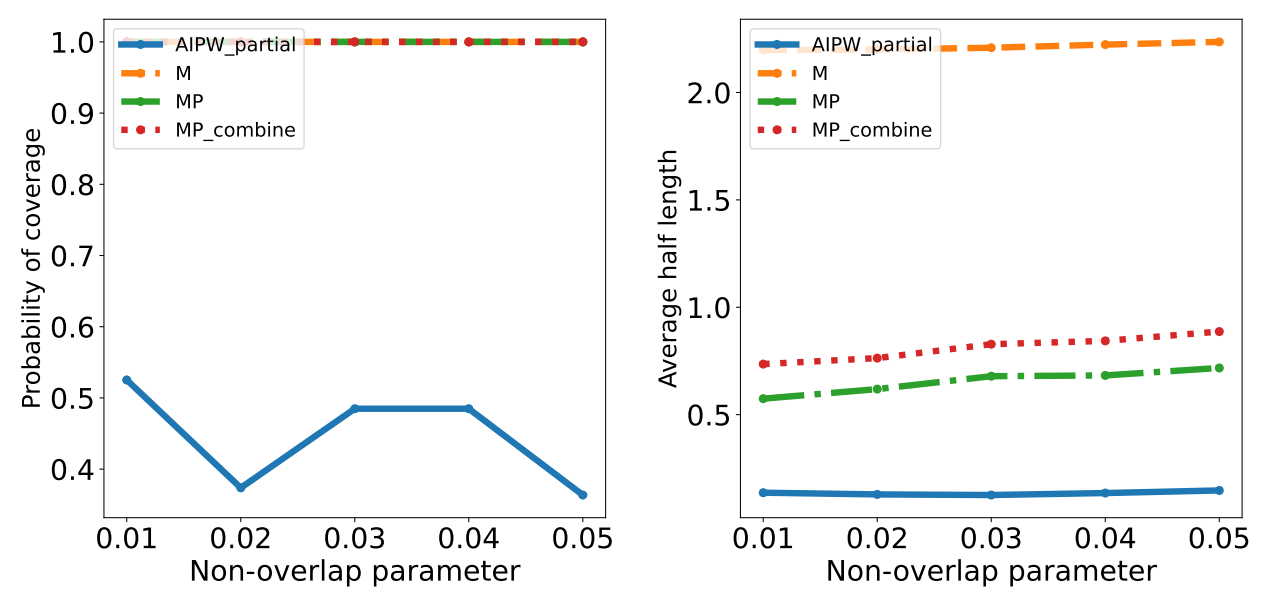


Figure 13. Probability of coverage and half length for MP and AlPW_{partial} with L=0.32, as we vary the non-overlap parameter η . Results are averaged over 100 runs. The larger the non-overlap parameter, the larger the non-overlap region is. The truncation threshold is always chosen to be the one such that AlPW_{partial} has the smallest length. We can see how unreliable AlPW_{partial} is and how our method MP can help mitigate it.

Sensitivity framework In contrast, our sensitivity approach provides a conservative and valid analysis of the bias induced by the truncation. In Figure 12, we show MP_{ϵ} across different values of the Lipschitz constant L and see that it successfully covers τ_{-} for $L = \hat{L}_{0.8}$ estimated from the overlap region (3.2). The confidence intervals MP_{ϵ} are wider than those produced by $\mathsf{AIPW}_{\mathsf{partial}}$, reflecting the conservative nature of minimax-type procedures, which explicitly account for the worst-case uncertainty due to extrapolation from the overlap region.

We also visualize the combined interval $MP_{combine}$ on the right side of Figure 12. As expected, $MP_{combine}$ intervals are wider than those from MP alone, since they aim to cover the full ATE τ rather than only τ_{-} in the non-overlap region. This increased width is a necessary trade-off to ensure coverage of the entire target estimand. Still, $MP_{combine}$ remains substantially more efficient than the fully conservative minimax confidence interval M, as it exploits the strengths of both the asymptotic method (in regions with good support) and the minimax method (in regions with poor overlap).

Coverage probabilities of confidence intervals To assess extrapolability, we contextualize the Lipschitz constant L in the right panel of Figure 7, and observe that the underlying CATE function is much smoother than in our simulation example due to the higher-dimensional nature of the covariates. Taking the 95th percentile Lipschitz parameter, we study the coverage probability of specific confidence intervals in Figure 13. Probability of coverage for AIPW_{partial} is highly sensitive to the degree of overlap in the data. As the degree of non-overlap increases, its coverage probability deteriorates substantially, indicating a higher risk of undercoverage and, consequently, misleading inference. On the other hand, our method MP, which leverages the minimax framework over the non-overlap region, offers a more robust estimate of the bias of AIPW_{partial}. Across all sce-

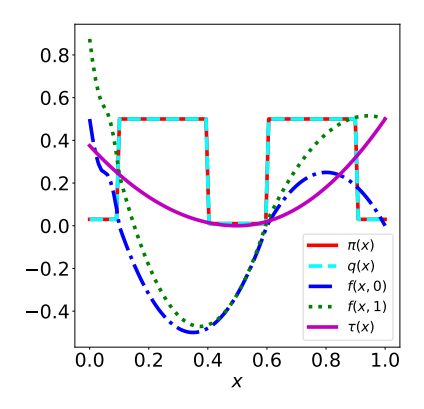


Figure 14: Simulation data collection setup

narios tested, MP achieves full (100%) coverage of the non-overlap region estimand τ_{-} . Similarly, MP_{combine} consistently achieves valid coverage for the full ATE τ , while remaining considerably narrower than the fully conservative interval generated by the naive minimax method M. This illustrates a key strength of our framework: it balances the need for robust inference in low-overlap regions with the desire for efficiency where data support is strong.

5 Guiding data collection

The notion of overlap studied in this work can potentially have implications beyond observational analysis. We explore one such scenario where the analyst may collect additional outcome data from units in the non-overlap region, so that the non-overlap region shrinks over time. Given some budget to assign treatments z_i to certain sample i, the realization of the updated treatment $\tilde{Z}_i(r)$ that depends on the sampling option r yields the updated outcome \tilde{Y}_i . We provide preliminary ideas where the notion of overlap we study can guide which batch of samples to collect.

5.1 Data collection

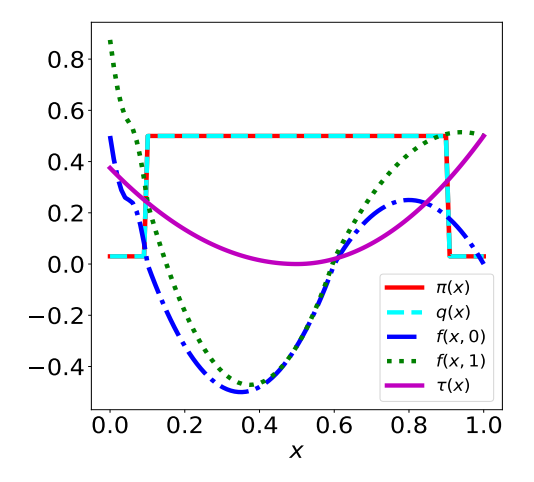
As a starting point, we focus on a simple scenario where the analyst already has two options in mind and needs to decide which one to proceed with. For each sampling option r, we can define the data

$$\widetilde{\mathcal{D}}(r) := \left\{ x_i, \widetilde{\pi}_i(r), \widetilde{Z}_i(\widetilde{\pi}_i(r)) \right\}_{i=1}^n,$$

as the realized data containing the updated treatment information, where $\tilde{\pi}_i(r)$ denotes the updated propensity score for unit i under option r. Note that the dataset $\tilde{\mathcal{D}}(r)$ does not involve Y and therefore can be computed prior to the actual sampling. This is because our approach explicitly considers all possible outcome functions instead of relying on the actual observed Y data. We can then compare different sampling options through

$$\mathbb{E}_{Z}\left[T\left(\mathsf{MP}_{\epsilon}\left(\widetilde{\mathcal{D}}(r)\right)\right)\right] \tag{5.1}$$

for some ϵ , where $T(\cdot)$ is the length of the interval MP and the expectation is taken over the randomness in Z. For a fixed ϵ , the metric (5.1) estimates the expected uncertainty of regions with $q(x) < \epsilon$ after the additional sampling.



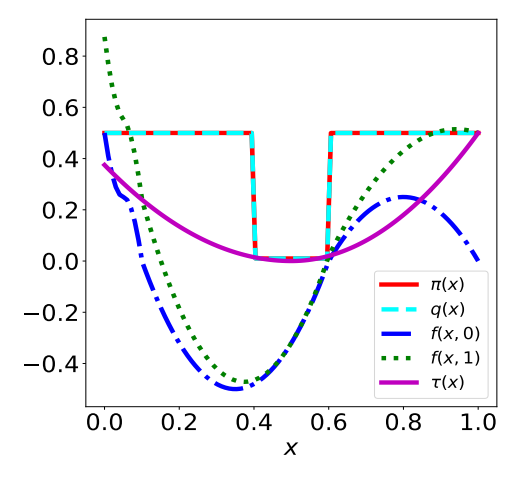


Figure 15. Left/right: after Option_1/Option_2, the distribution of $\pi(X)$. Option_1 is to collect data if $x \in \mathcal{X}_2 = (0.4, 0.6)$ and Option_2 is to collect data if $x \in \mathcal{X}_2 = (0, 0.1) \cup (0.9, 1)$. Option_1 appears better from the propensity score perspective (after sampling, the propensity score is 0.03 for Option_1 vs 0.01 for Option_2). As we can see later, Option_2 is the better option.

The simulation setup for this setting is depicted in Figure 14. We randomly sample n=500 points as the initial data. We imagine a scenario, with certain operational constraints being present, the analyst faces two feasible sampling options to collect new data, as depicted in Figure 15: $\mathtt{Option_1}$ is to collect data if $x \in \mathcal{X}_2 = (0.4, 0.6)$ and $\mathtt{Option_2}$ is to collect data if $x \in \mathcal{X}_2 = (0,0.1) \cup (0.9,1)$. In addition, we consider another policy \mathtt{Oracle} that samples all data $x \in \mathcal{X}_1 \cup \mathcal{X}_2$, which is the entire region without overlap, with probability 50% for each point. Therefore, the total number of data points that can be sampled are roughly the same for all three options. As we see later, the policy \mathtt{Oracle} performs well since it minimizes the region of limited overlap, but such random sampling may not always be feasible in practice. If the analyst decides to collect some data x_i , we assume she can set $\pi(x_i) = \frac{1}{2}$.

Option_1 and Option_2, the two sampling options, are nearly identical solely based on propensity scores as the propensity scores in these regions are nearly the same. This makes the options hard to distinguish, especially in high-dimensional feature spaces. However, we know intuitively from Figure 15 that Option_2 is better, as Option_1 samples data that can be extrapolated more easily from existing data: both the data from $x \in [0.1, 0.4]$ and $x \in [0.6, 0.9]$ can be used to infer the values for $x \in [0.4, 0.6]$, so the extra value of sampling these points is smaller compared to that in Option_2. Therefore, under Option_2, we need to perform less unreliable extrapolation, which is further reduced under Oracle.

Option	L = 4.28	L = 5.48	L = 6.65	L = 13.11
$Option_{-}1$	0.0958	0.1003	0.1046	0.1283
Option_2	0.0213	0.0242	0.0271	0.0430
Oracle	0.0117	0.0126	0.0134	0.0179

Table 1. Comparing three sampling options fixing $\epsilon = 0.04$. The Lipschitz constants correspond to \tilde{L}_p (3.2) for $p \in \{0.8, 0.85, 0.9, 0.95\}$. Given the data is coming from Figure 14, the choice of $\epsilon = 0.04$ is not important, as any $\epsilon < 0.1$ yields the same weight w_{ϵ} , and hence the same result. We conduct 10 runs of Z to estimate (5.1) and only report the mean as the variance is nearly zero. We observe consistent rankings across different options for different choices of L.

To formalize the above intuition, we compute our metric (5.1) for each of the three options and report them in Table 1 over different Lipschitz constants. Similar to Figure 7, we perform contextualization and use Lipschitz constants taking values \tilde{L}_p (3.2) for $p \in \{0.8, 0.85, 0.9, 0.95\}$. Our approach formally considers the extrapolability of outcome functions and designs sampling evaluation based on this. Therefore, our metric predicts that Option_2 is better. To complement the worst-case analysis in Table 1, we then evaluate these two options by repeatedly sampling according to these options and report the error (the distance between the CI and the estimand) of the resulting CI generated by AIPW_{partial} in Table 2.

Option	Coverage of AIPW _{partial}	Distance of AIPW _{partial}
$Option_{-}1$	0.051 ± 0.0136	0.0182 ± 0.0006
Option_2	0.901 ± 0.0185	0.0009 ± 0.0002
Oracle	0.985 ± 0.0075	0.00009 ± 0.00006

Table 2. Same setting as Table 1. Comparing two sampling options fixing $\epsilon = 0.04$. The error of AIPW_{partial} is also computed using 200 runs and also include standard errors. Compared with Table 1, our metric successfully predicts the ranking of different sampling options.

5.2 Confidence sequence

Our framework is also applicable when the analyst conducts continual sampling/data collection with an arbitrary stopping policy, and we defer those results to Appendix D.3. From Figure 16, we observe how the uncertainty over τ_{-} keeps reducing as the level of limited overlap reduces, and we offer the analyst a flexible way to specify the stopping rule for sampling subject to a given sampling budget.

Theoretically, guiding continual data collection requires generalizing the coverage guarantee in (2.3) to a uniform coverage property:

$$\inf_{f \in \mathcal{F}} \mathbb{P}_f \left(\tau_{\boldsymbol{w}_t}(f) \in \mathcal{C}_t, \, \forall t \ge 1 \right) \ge 1 - \alpha. \tag{5.2}$$

In particular, this setting includes problems where $\tau_{\boldsymbol{w}_t}(f)$ varies over time as the non-overlap region evolves with new data. Since the stopping time is not fixed in advance, a naive union bound based on a pre-specified horizon T does not provide valid coverage for arbitrary, data-dependent stopping rules. Instead, we require a confidence sequence. We assume the analyst conducts continual sampling and that, at every time t, new data will be collected. At each time t, one solves the problem (2.10) and finds an estimator $\hat{\tau}_t = \boldsymbol{w}_t^{\top} \boldsymbol{y}_t$ at t to estimate $\tau_{\boldsymbol{w}_t}(f)$, which is a linear combination of the data, and \boldsymbol{y}_t is the outcome data at time t. As we will show in Lemma 6, \mathcal{C}_t , which generalizes (2.6), is a valid confidence sequence:

$$C_t = \hat{\tau}_t \pm \operatorname{sd}(\hat{\tau}_t) \operatorname{cv}_{\alpha_t} \left(\frac{\overline{\operatorname{bias}}_t(\hat{\tau}_t)}{\operatorname{sd}(\hat{\tau}_t)} \right), \qquad \alpha_t := \frac{6\alpha}{\pi^2 t^2}.$$
 (5.3)

In addition, $\operatorname{sd}(\hat{\tau}_t)$ can be computed by noting that $\hat{\tau}_t = \boldsymbol{w}_t^{\top} \boldsymbol{y}_t$ and $\overline{\operatorname{bias}}_t(\hat{\tau}_t)$ is given by (2.7).

6 Discussion

This paper develops a practical minimax-based approach for reliable treatment effect inference in scenarios with limited covariate overlap between treated and control groups. By extrapolating the

outcome function over the covariate space, our framework produces robust confidence intervals for treatment effects in regions without overlap and mitigates the bias introduced by common practices such as data trimming. Additionally, it serves as a diagnostic tool for identifying subpopulations with limited effective sample sizes and offers principled guidance for addressing challenges associated with poor overlap. Experimental results, across both simulated and real-world datasets, demonstrate the framework's effectiveness in improving the reliability and interpretability of treatment effect inference.

A key feature of our approach is a sensitivity framework that allows analysts to systematically quantify the uncertainty associated with extrapolating from well-supported (overlap) regions to sparse (non-overlap) regions. By parameterizing the smoothness of the outcome function class via a Lipschitz constant (see (2.12)), our method enables users to assess how assumptions on function regularity influence the resulting confidence intervals. This sensitivity analysis is operationalized through a data-driven contextualization procedure, which calibrates the Lipschitz constant based on observed covariates and outcomes in the overlap region. The result is a transparent, interpretable trade-off between bias and extrapolation strength—allowing analysts to probe, validate, and communicate the robustness of their causal conclusions.

In practice, analysts often have more domain-specific knowledge about outcome smoothness or structural relationships in the data. Incorporating this knowledge into the function class can sharpen inference and reduce conservativeness in extrapolated intervals. Moreover, the sensitivity framework highlights how minimal deviations in smoothness assumptions can affect bias due to trimming, helping practitioners avoid spurious certainty in under-supported regions.

An exciting direction for future work is extending this framework to off-policy evaluation tasks with richer action spaces (e.g., multi-armed treatments). Such settings require imputing multiple counterfactuals per unit, increasing both the complexity of the function class and the difficulty of computing the associated modulus of continuity. Developing scalable and efficient methods to handle this will be crucial for broader adoption of the minimax approach in high-stakes applications.

References

- [1] A. Abadie and G. W. Imbens. Large sample properties of matching estimators for average treatment effects. *Econometrica*, 74(1):235–267, 2006.
- [2] A. Abadie and G. W. Imbens. Bias-corrected matching estimators for average treatment effects. Journal of Business & Economic Statistics, 29(1):1–11, 2011.
- [3] T. B. Armstrong and M. Kolesár. Optimal inference in a class of regression models. *Econometrica*, 86(2):655–683, 2018.
- [4] T. B. Armstrong and M. Kolesár. Finite-sample optimal estimation and inference on average treatment effects under unconfoundedness. *Econometrica*, 89(3):1141–1177, 2021.
- [5] G. Beliakov. Interpolation of Lipschitz functions. *Journal of Computational and Applied Mathematics*, 196(1):20–44, 2006.
- [6] M. Busso, J. DiNardo, and J. McCrary. New evidence on the finite sample properties of propensity score reweighting and matching estimators. The Review of Economics and Statistics, 96 (5):885–897, 2014.

- [7] T. T. Cai and M. G. Low. An adaptation theory for nonparametric confidence intervals. *The Annals of statistics*, 32(5):1805–1840, 2004.
- [8] V. Chernozhukov, D. Chetverikov, M. Demirer, E. Duflo, C. Hansen, W. Newey, and J. Robins. Double/debiased machine learning for treatment and structural parameters. *The Econometrics Journal*, 21(1):C1–C68, 2018.
- [9] S. R. Cole and M. A. Hernán. Constructing Inverse Probability Weights for Marginal Structural Models. *American Journal of Epidemiology*, 168(6):656–664, 2008.
- [10] R. K. Crump, V. J. Hotz, G. W. Imbens, and O. A. Mitnik. Moving the goalposts: Addressing limited overlap in the estimation of average treatment effects by changing the estimand. Technical report, National Bureau of Economic Research, 2006.
- [11] R. K. Crump, V. J. Hotz, G. W. Imbens, and O. A. Mitnik. Dealing with limited overlap in estimation of average treatment effects. *Biometrika*, 96(1):187–199, 2009.
- [12] Y. Cui. Individualized Decision-Making Under Partial Identification: Three Perspectives, Two Optimality Results, and One Paradox. *Harvard Data Science Review*, (3), 2021.
- [13] R. H. Dehejia and S. Wahba. Causal effects in nonexperimental studies: Reevaluating the evaluation of training programs. *Journal of the American Statistical Association*, 94(448): 1053–1062, 1999.
- [14] D. L. Donoho. Statistical estimation and optimal recovery. Annals of Statistics, 22(1):238–270, 1994.
- [15] A. D'Amour, P. Ding, A. Feller, L. Lei, and J. Sekhon. Overlap in observational studies with high-dimensional covariates. *Journal of Econometrics*, 221(2):644–654, 2021.
- [16] M. Frölich. Finite-sample properties of propensity-score matching and weighting estimators. Review of Economics and Statistics, 86(1):77–90, 2004.
- [17] R. J. Glynn, M. Lunt, K. J. Rothman, C. Poole, S. Schneeweiss, and T. Stürmer. Comparison of alternative approaches to trim subjects in the tails of the propensity score distribution. *Pharmacoepidemiology and drug safety*, 2019.
- [18] J. J. Heckman, H. Ichimura, and P. E. Todd. Matching As An Econometric Evaluation Estimator: Evidence from Evaluating a Job Training Programme. *The Review of Economic Studies*, 64(4):605–654, 10 1997.
- [19] P. Heiler and E. Kazak. Valid inference for treatment effect parameters under irregular identification and many extreme propensity scores. *Journal of Econometrics*, 222(2), 2021.
- [20] H. Hong, M. P. Leung, and J. Li. Inference on finite-population treatment effects under limited overlap. *The Econometrics Journal*, 23(1):32–47, 2019.
- [21] S. R. Howard, A. Ramdas, J. McAuliffe, and J. Sekhon. Time-uniform, nonparametric, nonasymptotic confidence sequences. *The Annals of Statistics*, 49, 2021.
- [22] Z. Hussain, M. Oberst, M.-C. Shih, and D. Sontag. Falsification before extrapolation in causal effect estimation. In *Proceedings of the 36th International Conference on Neural Information*

- Processing Systems, 2022. ISBN 9781713871088.
- [23] Z. Hussain, M.-C. Shih, M. Oberst, I. Demirel, and D. Sontag. Falsification of internal and external validity in observational studies via conditional moment restrictions. In *Proceedings of The 26th International Conference on Artificial Intelligence and Statistics*, pages 5869–5898, 2023.
- [24] G. Imbens. Nonparametric estimation of average treatment effects under exogeneity: a review. *The Review of Economics and Statistics*, 86(1):4–29, 2004.
- [25] G. W. Imbens and C. F. Manski. Confidence intervals for partially identified parameters. *Econometrica*, 72(6):1845–1857, 2004.
- [26] C. Ju, J. Schwab, and M. J. van der Laan. On adaptive propensity score truncation in causal inference. *Statistical methods in medical research*, 2019.
- [27] A. B. Juditsky and A. S. Nemirovski. Nonparametric estimation by convex programming. *The Annals of Statistics*, 37:2278 2300, 2009.
- [28] N. Kallus. Generalized optimal matching methods for causal inference. *Journal of Machine Learning Research*, 21(62):1–54, 2020.
- [29] N. Kallus and A. Zhou. Minimax-optimal policy learning under unobserved confounding. Management Science, 67(5):2870–2890, 2021.
- [30] J. D. Y. Kang and J. L. Schafer. Demystifying Double Robustness: A Comparison of Alternative Strategies for Estimating a Population Mean from Incomplete Data. Statistical Science, 22(4):523 539, 2007.
- [31] S. Khan and D. Nekipelov. On uniform inference in nonlinear models with endogeneity. *Journal of Econometrics*, 240(2):105261, 2024.
- [32] S. Khan and E. Tamer. Irregular identification, support conditions, and inverse weight estimation. *Econometrica*, 78(6):2021–2042, 2010.
- [33] S. Khan, M. Saveski, and J. Ugander. Off-policy evaluation beyond overlap: Sharp partial identification under smoothness. In *Proceedings of the 41st International Conference on Machine Learning*, volume 235, pages 23734–23757, 2024.
- [34] R. Koenker and Y. Bilias. Quantile regression for duration data: A reappraisal of the pennsylvania reemployment bonus experiments. In *Economic applications of quantile regression*, pages 199–220. Springer, 2002.
- [35] R. J. LaLonde. Evaluating the econometric evaluations of training programs with experimental data. *The American Economic Review*, 76(4):604–620, 1986.
- [36] O. Landgren, D. S. Siegel, D. Auclair, A. Chari, M. Boedigheimer, T. Welliver, K. Mezzi, K. Iskander, and A. Jakubowiak. Carfilzomib-lenalidomide-dexamethasone versus bortezomib-lenalidomide-dexamethasone in patients with newly diagnosed multiple myeloma: results from the prospective, longitudinal, observational commpass study. *Blood*, 132:799, 2018.
- [37] B. K. Lee, J. Lessler, and E. A. Stuart. Weight trimming and propensity score weighting.

- PLOS ONE, 6(3):1-6, 03 2011.
- [38] B. Li, K. Ren, L. Shen, P. Hou, Z. Su, A. Di Bacco, J.-L. Hong, A. Galaznik, A. B. Dash, V. Crossland, P. Dolin, and S. Szalma. Comparing bortezomib-lenalidomide-dexamethasone (vrd) with carfilzomib-lenalidomide-dexamethasone (krd) in the patients with newly diagnosed multiple myeloma (ndmm) in two observational studies. *Blood*, 132:3298, 2018.
- [39] F. Li, L. E. Thomas, and F. Li. Addressing Extreme Propensity Scores via the Overlap Weights. *American Journal of Epidemiology*, 188(1):250–257, 2018.
- [40] X. Ma and J. Wang. Robust inference using inverse probability weighting. *Journal of the American Statistical Association*, 115(532):1851–1860, 2020.
- [41] Y. Ma, P. H. Sant'Anna, Y. Sasaki, and T. Ura. Doubly robust estimators with weak overlap. arXiv:2304.08974 [stat.ME], 2023.
- [42] C. F. Manski. Nonparametric bounds on treatment effects. The American Economic Review, 80(2):319–323, 1990.
- [43] NIH. Relating clinical outcomes in multiple myeloma to personal assessment of genetic profile(com-mpass), 2016. URL https://clinicaltrials.gov/study/NCT01454297.
- [44] M. L. Petersen, K. E. Porter, S. Gruber, Y. Wang, and M. J. van der Laan. Diagnosing and responding to violations in the positivity assumption. *Statistical Methods in Medical Research*, 21(1):31–54, 2012.
- [45] P. R. Rosenbaum and D. B. Rubin. The central role of the propensity score in observational studies for causal effects. *Biometrika*, 70(1):41–55, 1983.
- [46] C. Rothe. Robust confidence intervals for average treatment effects under limited overlap. *Econometrica*, 85(2):645–660, 2017.
- [47] Y. Sasaki and T. Ura. Estimation and inference for moments of ratios with robustness against large trimming bias. *Econometric Theory*, 38(1):66–112, 2022.
- [48] M. H. Schneider and S. A. Zenios. A comparative study of algorithms for matrix balancing. *Operations Research*, 38(3), 1990.
- [49] J. A. Smith and P. E. Todd. Does matching overcome LaLonde's critique of nonexperimental estimators? *Journal of Econometrics*, 125:305–353, 2005.
- [50] J. Stoye. More on confidence intervals for partially identified parameters. *Econometrica*, 77 (4):1299–1315, 2009.
- [51] T. Stürmer, K. J. Rothman, J. Avorn, and R. J. Glynn. Treatment effects in the presence of unmeasured confounding: dealing with observations in the tails of the propensity score distribution—a simulation study. *American Journal of Epidemiology*, 172(7):843–854, 2010.
- [52] S. Yang and P. Ding. Asymptotic inference of causal effects with observational studies trimmed by the estimated propensity scores. *Biometrika*, 105(2):487–493, 2018.

A Proof of Lemma 1

In this section, we closely follow the notation in [4]. We let $n_1 = |\{i : z_i = 1\}|$ and $n_0 = |\{i : z_i = 0\}|$ denote the total number of samples with z = 1 and z = 0. With slight abuse of notation, we let $i \in [n_1]$ denote the *i*-th sample for those with $z_i = 1$ and similarly write $j \in [n_0]$ to denote the *j*-th sample for those with $z_i = 0$.

We first define $m_i = (2z_i - 1)f(x_i, z_i)$, and $r_i = (1 - 2z_i)f(x_i, 1 - z_i)$. Then Armstrong and Kolesár [4] has shown that the modulus of continuity (2.4) can be written as

$$\min_{f \in \mathcal{F}_L} \frac{1}{2} \sum_{i=1}^n \frac{f^2(x_i, z_i)}{\sigma^2(x_i, z_i)} - \mu \tau_{\boldsymbol{w}}(f) / L = \min_{f \in \mathcal{F}_L} \frac{L^2}{2} \sum_{i=1}^n \frac{f^2(x_i, z_i)}{\sigma^2(x_i, z_i)} - \mu \tau_{\boldsymbol{w}}(f), \tag{A.1}$$

which can be further written as

$$\frac{1}{2} \sum_{i=1}^{n} \frac{m_i^2}{\sigma^2(z_i)} - \mu \left(\sum_{i=1}^{n} w_i(m_i + r_i) \right) + \sum_{i,j: \ z_i = 1 - z_j = 1} \left[\Lambda_{ij}^0(r_i - m_j - ||x_i - x_j||) + \Lambda_{ij}^1(r_j - m_i - ||x_i - x_j||) \right]. \tag{A.2}$$

where $\Lambda_{ij}^0, \Lambda_{ij}^1 \geq 0$ are the optimal dual variables for the Lipschitz constraints.

Now we are ready to prove a stronger version of Lemma 1.

Lemma 3. Let $\mu \geq 0$ and $\Lambda \geq 0$ be optimal dual variables corresponding to the Lipschitz constraints (2.12). We can rewrite $\hat{\tau}_{\delta_{\text{FLCI}}}(\boldsymbol{w})$ (2.5) as

$$\hat{\tau}_{\delta_{\text{FLCI}}}(\boldsymbol{w}) = \sum_{k=1}^{n} \left[\mathcal{I}\left(z_{k}=0\right) \left(\sum_{i:z_{i}=1} \frac{\Lambda_{ik}^{1}}{\mu} y_{i} - w_{k} y_{k} \right) + \mathcal{I}\left(z_{k}=1\right) \left(w_{k} y_{k} - \sum_{j:z_{j}=0} \frac{\Lambda_{kj}^{0}}{\mu} y_{j} \right) \right] \mathcal{I}\left(w_{k} > 0\right),$$
(A.3)

Thus, the minimax estimator will impute the counterfactual values as

$$w_k \hat{f}(x_k, 1 - z_k) = \sum_{j: z_j = 1 - z_k} W_{jk} y_j \quad \text{where} \quad W_{jk} = \begin{cases} \frac{\Lambda_{jk}^1}{\mu}, & \text{if } z_k = 0\\ \frac{\Lambda_{kj}^0}{\mu}, & \text{if } z_k = 1. \end{cases}$$
(A.4)

If
$$z_k = 0$$
, then $\sum_i \frac{\Lambda_{ik}^1}{\mu} = w_k$; if $z_k = 1$, then $\sum_j \frac{\Lambda_{kj}^0}{\mu} = w_k$.

Proof [Proof of Lemma 3] We let $f_i = f^*(x_i, z_i)$ denote the optimal solution of (2.4) and $m_i = (2z_i - 1)f_i$, $r_i = (1 - 2z_i)f_i$. We also let $\mu, \Lambda^0_{ij}, \Lambda^1_{ij}$ denote the optimal dual variable. Note that at the optimal solution, the conic constraint must be binding so that $\mu > 0$. Fix k and suppose $z_k = 0$, from (2.5), we need to show that

$$-w_k - \sum_{i \in [n_1]} \frac{\Lambda_{ik}^0}{\mu} = \left(\sum_{i=1}^n w_i\right) \frac{f_k}{\sum_{i \in [n_1]} f_i}.$$
 (A.5)

The proof for the case with $z_k = 1$ is similar thus omitted. From (S1) of Section D.2 in [4], we have

$$\frac{m_j}{\sigma^2} = \mu w_j + \sum_{i \in [n_1]} \Lambda_{ij}^0, \forall j \in [n_0]$$

so that

$$\frac{m_j}{\sigma^2 \mu} = w_j + \sum_{i \in [n_1]} \frac{\Lambda_{ij}^0}{\mu}, \forall j \in [n_0]. \tag{A.6}$$

From [4], we know

$$\frac{m_i}{\sigma^2} = \mu w_i + \sum_{j \in [n_0]} \Lambda_{ij}^1, \forall i \in [n_1]. \tag{A.7}$$

Summing over (A.7), we have

$$\sum_{i \in [n_1]} \frac{m_i}{\sigma^2} = \sum_{i \in [n_1]} w_i \mu + \sum_{j \in [n_0]} \sum_{i \in [n_1]} \Lambda^1_{ij}.$$

Since $\sum_{i \in [n_1]} \Lambda_{ij}^1 = \mu w_j$ from [4], we have

$$\sum_{i \in [n_1]} \frac{m_j}{\sigma^2} = \sum_{i \in [n_1]} w_i \mu + \sum_{i \in [n_1]} \sum_{j \in [n_0]} \Lambda_{ij}^1 = \sum_{i \in [n_1]} w_i \mu + \sum_{j \in [n_0]} w_j \mu = \left(\sum_{i=1}^n w_i\right) \mu. \tag{A.8}$$

Therefore, we arrive at

$$-w_k - \sum_{i \in [n_1]} \frac{\Lambda_{ik}^0}{\mu} = -\frac{m_k}{\sigma^2 \mu} = \frac{f_k}{\sigma^2 \mu} = \left(\sum_{i=1}^n w_i\right) \frac{f_k}{\sum_{i \in [n_1]} f_i},$$

where the first equality follows from (A.6), the second one follows from $m_k = -f_k$ as $z_k = 0$, and the last one follows from (A.6). Thus, we show (A.5) and finish the proof.

B Computation of $\omega_{\mathcal{F};\mathcal{D}}(\delta)$

We follow [4]'s procedure to compute $\omega_{\mathcal{F};\mathcal{D}}(\delta)$. Most of the components there are directly applicable. However, one key component in [4]'s procedure is to solve a problem that involves finding a matrix with given row and column sum constraints and certain entries of the matrix must be zero, i.e., Step 2(b) in Section A.3 of [4]. The implementation approach in [4], which uses matrix inversion, may be slow to ensure dual feasibility $\Lambda^d \geq 0$ and thus may need many iterations to arrive at a solution. Instead, we solve the problem by converting it into a max flow algorithm (Algorithm 1) instance following [48], which can be more efficient than using matrix inversion.

C Details of analytical insights

In this section, we provide details and proofs of results in Section 2.3. We start by proving Lemma 2.

C.1 Proof of Lemma 2

Fix L and δ . Let f^* be an optimal solution of the program (2.18). We write

$$f_{i,1} := f^*(x_i, 1), \qquad f_{i,0} := f^*(x_i, 0),$$

Algorithm 1 $MAX_FLOW(p, q, E)$

- 1: **Input:** Row sums $p = [p_1, p_2, \dots, p_m]$, Column sums $q = [q_1, q_2, \dots, q_n]$, Allowed indices E
- 2: **Output:** A matrix $A \geq 0$ that satisfies $A_{ij} = 0$ if $(i, j) \notin E$ and $\sum_j A_{ij} = p_i$ for all i and $\sum_i A_{ij} = q_j$ for all j.
- 3: Create a directed graph G_f with a source node s and a sink node t
- 4: **for** each row i **do**
- 5: Create a node n_i
- 6: Add an edge from s to n_i with capacity p_i
- 7: end for
- 8: **for** each column j **do**
- 9: Create a node n_i
- 10: Add an edge from n_j to t with capacity q_j
- 11: end for
- 12: **for** each index $(i, j) \in E$ **do**
- 13: Add an edge from n_i to n_j with capacity ∞
- 14: end for
- 15: Compute the maximum flow from s to t in the graph G_f with costs c=1
- 16: **return** Matrix A with entries $A_{ij} = f_{n_i,n_j}$, where f_{n_i,n_j} is the flow from node n_i to n_j .

and define

$$d_{i,j} := L|x_i - x_j|.$$

Let

$$W_{+} := \{i : w_{i} > 0\}, \qquad W_{-} := \{i : w_{i} = 0\}$$

denote the sets of points with and without weights, respectively.

Step 1: Nonnegativity of $f_{i,1}$. We first show that for every i with $z_i = 1$, we can assume that

$$f_{i,1} \ge 0.$$
 (C.1)

Indeed, suppose there exists an index i with $z_i = 1$ and $f_{i,1} < 0$. Define a new solution \hat{f} by

$$\hat{f}_{i,1} := \max\{f_{i,1}, 0\}$$
 for all i with $z_i = 1$,

and keep all other coordinates (including all $f_{i,0}$) unchanged. By construction, and since the map $x \mapsto \max\{x,0\}$ is 1-Lipschitz,

$$|\hat{f}_{i,1} - \hat{f}_{j,1}| = |\max\{f_{i,1}, 0\} - \max\{f_{j,1}, 0\}| \le |f_{i,1} - f_{j,1}| \le d_{i,j}$$
 for all i, j .

Thus, the Lipschitz constraints remain feasible. Moreover, because the objective of (2.18) only depends on $f_{i,1}$ at weighted points $i \in W_+$ and these have $w_i > 0$ with $z_i = 1$, increasing a negative $f_{i,1}$ to 0 weakly *improves* the objective (while keeping feasibility). So we may assume (C.1) without loss of generality.

Step 2: Ordering the zero-weight points by distance. For $i \in W_-$, define its distance to the positive-weight region by

$$\eta_i := \min\{ |x_i - x_j| : j \in W_+ \}.$$

Order the indices in W_{-} so that

$$\eta_1 \leq \eta_2 \leq \cdots \leq \eta_m$$

where $\{1, \ldots, m\} = W_{-}$ after relabeling. Our goal is to construct another optimal solution g such that

$$i < j \implies \eta_i \le \eta_j \text{ and } g_{i,1} \ge g_{j,1},$$
 (C.2)

i.e., among points in W_- , the map $i \mapsto g_{i,1}$ is weakly decreasing as the distance η_i grows.

Step 3: Trouble points and one-step modification. Starting from the fixed optimal solution f^* , we work only with the coordinates $f_{i,1}$ for $i \in W_-$; all other coordinates $(i \in W_+ \text{ and all } f_{i,0})$ will never be changed.

Call an index $k \in \{1, \dots, m-1\}$ a trouble point if

$$\eta_k \le \eta_{k+1} \quad \text{but} \quad f_k < f_{k+1}.$$
(C.3)

If there is no trouble point, then (C.2) already holds with $g_{i,1} = f_{i,1}$ and we are done. Otherwise, let i^* be the smallest index that satisfies (C.3).

Given such an i^* , consider all zero-weight points that are at least as far as i^* and whose value is too large, namely

$$\mathcal{I} := \{ j \in W_{-} : \eta_{j} \ge \eta_{i^{*}}, \ f_{j,1} > f_{i^{*},1} \}.$$
(C.4)

Define a modified solution g by

$$g_j := \begin{cases} f_{i^*,1}, & j \in \mathcal{I}, \\ f_{j,1}, & j \notin \mathcal{I}, \end{cases}$$

and keep $g_{i,0} = f_{i,0}$ for all i. In words, we leave every weighted point $i \in W_+$ unchanged, and among W_- we replace the values at the indices in \mathcal{I} by $f_{i^*,1}$ (which is smaller), while leaving all other coordinates unchanged.

Step 4: Feasibility and optimality of the modified solution. We check that g is feasible and optimal for (2.18).

- (i) Objective value. By definition of W_+ and W_- , the objective depends only on $f_{i,1}$ with $i \in W_+$. Since we never changed those coordinates, g has exactly the same objective value as f^* and is therefore also optimal.
 - (ii) Lipschitz constraints. For any pair (p,q) we must show that

$$|g_{p,1} - g_{q,1}| \le d_{p,q}$$
.

The original f satisfied $|f_{p,1} - f_{q,1}| \leq d_{p,q}$ for all p,q. We compare old and new values case by case:

- If $p, q \notin \mathcal{I}$, then $g_{p,1} = f_{p,1}$ and $g_{q,1} = f_{q,1}$, so the constraint is unchanged.
- If $p, q \in \mathcal{I}$, then $g_{p,1} = g_{q,1} = f_{i^*,1}$ and therefore

$$|g_{p,1} - g_{q,1}| = 0 \le d_{p,q}$$
.

• If $p \in \mathcal{I}$ and $q \notin \mathcal{I}$, then

$$|g_{p,1} - g_{q,1}| = |f_{i^*,1} - f_{q,1}|.$$

By construction of \mathcal{I} (C.4), $f_{i^*,1} \leq f_{p,1}$ for every $p \in \mathcal{I}$. There are two cases:

1. If $q \in W_+$, then we have $d_{i^*,q} \leq d_{p,q}$ so that

$$|g_{p,1} - g_{q,1}| = |f_{i^*,1} - f_{q,1}| \le d_{i^*,q} \le d_{p,q}.$$

2. If $q \in W_-$, $\eta_q \leq \eta_{i^*}$, i.e., i^* is in the middle of p and q, then we also have $d_{i^*,q} \leq d_{p,q}$ so that

$$|g_{p,1} - g_{q,1}| = |f_{i^*,1} - f_{q,1}| \le d_{i^*,q} \le d_{p,q}$$

3. If $q \in W_-$, $\eta_q > \eta_{i^*}$, in this case, $q \notin \mathcal{I}$ implies $f_{q,1} \leq f_{i^*,1} \leq f_{p,1}$ so

$$|g_{p,1} - g_{q,1}| = |f_{i^*,1} - f_{q,1}| \le |f_{p,1} - f_{q,1}| \le d_{p,q}.$$

• If $p \notin \mathcal{I}$ and $q \in \mathcal{I}$, this is similar to the previous case.

Therefore g is feasible and optimal. In summary, we have constructed a solution g with

$$i < j \le i^* + 1 \implies \eta_i \le \eta_j \text{ and } g_{i,1} \ge g_{j,1},$$

Proceeding in the same way as above, we can remove all trouble points and we complete proving (C.2).

C.2 The example visualized in Section 2.3

In Lemma 5, we provide the details of the example visualized in Section 2.3, which is summarized in Figure 5 and Figure 6. Before discussing it, we present the following technical lemma which will be useful.

Lemma 4. Let $K \in \mathbb{R}^{n \times m}$ have full column rank and suppose the feasible set

$$S := \left\{ \boldsymbol{w} \in \mathbb{R}^n : \|\boldsymbol{w}\| \le R, \ \boldsymbol{K}^\top \boldsymbol{w} = \boldsymbol{d} \right\}$$

is nonempty. Define

$$oldsymbol{A} := oldsymbol{K}^{ op} oldsymbol{K}, \qquad oldsymbol{b} := oldsymbol{K}^{ op} oldsymbol{u}, \qquad \gamma := \|oldsymbol{u}\|^2,$$

and

$$w_0 := KA^{-1}d, \qquad \rho^2 := ||w_0||^2 = d^{\top}A^{-1}d.$$

Let

$$P := I - KA^{-1}K^{\top}$$

denote the orthogonal projector onto $\ker(\mathbf{K}^{\top})$. Then $\rho \leq R$ and

$$\max_{\boldsymbol{w} \in S} \left\{ \boldsymbol{u}^{\top} \boldsymbol{w} \right\} = \boldsymbol{u}^{\top} \boldsymbol{w}_0 + \| \boldsymbol{P} \boldsymbol{u} \| \sqrt{R^2 - \rho^2} = \boldsymbol{b}^{\top} \boldsymbol{A}^{-1} \boldsymbol{d} + \sqrt{\gamma - \boldsymbol{b}^{\top} \boldsymbol{A}^{-1} \boldsymbol{b}} \sqrt{R^2 - \boldsymbol{d}^{\top} \boldsymbol{A}^{-1} \boldsymbol{d}}.$$

Proof [Proof of Lemma 4] Define w_0 as the minimum-norm solution of the affine constraint:

$$w_0 := \arg \min\{\|w\| : K^\top w = d\}.$$

Solving the normal equations gives $w_0 = KA^{-1}d$ with $A = K^{\top}K$. Let

$$S_{\text{aff}} := \{ \boldsymbol{w} : \boldsymbol{K}^{\top} \boldsymbol{w} = \boldsymbol{d} \}.$$

Thus, every feasible $\mathbf{w} \in S_{\text{aff}}$ can be written uniquely as

$$oldsymbol{w} = oldsymbol{w}_0 + oldsymbol{z}, \qquad oldsymbol{z} \in \ker(oldsymbol{K}^{ op}).$$

Using this decomposition, the original problem is equivalent to

$$\max_{\boldsymbol{z} \in \ker(\boldsymbol{K}^{\top})} \left\{ \boldsymbol{u}^{\top}(\boldsymbol{w}_0 + \boldsymbol{z}) : \|\boldsymbol{w}_0 + \boldsymbol{z}\| \leq R \right\}.$$

Since $\boldsymbol{w}_0 \perp \ker(\boldsymbol{K}^\top)$, for every $\boldsymbol{z} \in \ker(\boldsymbol{K}^\top)$,

$$\|\boldsymbol{w}_0 + \boldsymbol{z}\|^2 = \|\boldsymbol{w}_0\|^2 + \|\boldsymbol{z}\|^2 = \rho^2 + \|\boldsymbol{z}\|^2.$$

The constraint $\|\boldsymbol{w}_0 + \boldsymbol{z}\| \leq R$ becomes

$$\|z\|^2 \le R^2 - \rho^2$$

so feasibility implies $\rho \leq R$. Moreover, for $z \in \ker(K^{\top})$,

$$\boldsymbol{u}^{\top} \boldsymbol{z} = (\boldsymbol{P} \boldsymbol{u})^{\top} \boldsymbol{z},$$

since P is the orthogonal projector onto $\ker(K^{\top})$. Thus the problem reduces to

$$\max_{\boldsymbol{z} \in \ker(\boldsymbol{K}^\top)} \left\{ \boldsymbol{u}^\top \boldsymbol{w}_0 + \boldsymbol{u}^\top \boldsymbol{z}, \|\boldsymbol{z}\| \leq \sqrt{R^2 - \rho^2} \right\} = \max_{\boldsymbol{z} \in \mathbb{R}^n} \left\{ \boldsymbol{u}^\top \boldsymbol{w}_0 + (\boldsymbol{P} \boldsymbol{u})^\top \boldsymbol{z}, \|\boldsymbol{z}\| \leq \sqrt{R^2 - \rho^2} \right\}.$$

Since

$$\max_{\|\boldsymbol{z}\| \leq \sqrt{R^2 - \rho^2}} (\boldsymbol{P} \boldsymbol{u})^\top \boldsymbol{z} = \|\boldsymbol{P} \boldsymbol{u}\| \sqrt{R^2 - \rho^2},$$

$$\max_{\boldsymbol{w} \in S} \boldsymbol{u}^{\top} \boldsymbol{w} = \boldsymbol{u}^{\top} \boldsymbol{w}_0 + \|\boldsymbol{P} \boldsymbol{u}\| \sqrt{R^2 - \rho^2}.$$

Finally, using $\boldsymbol{w}_0 = \boldsymbol{K} \boldsymbol{A}^{-1} \boldsymbol{d}$ and $\boldsymbol{P} = \boldsymbol{I} - \boldsymbol{K} \boldsymbol{A}^{-1} \boldsymbol{K}^{\top}$, we obtain

$$m{u}^{ op}m{w}_0 = m{b}^{ op}m{A}^{-1}m{d}, \quad \|m{P}m{u}\|^2 = \|m{u}\|^2 - m{b}^{ op}m{A}^{-1}m{b} = \gamma - m{b}^{ op}m{A}^{-1}m{b},$$

and $\rho^2 = \mathbf{d}^{\mathsf{T}} \mathbf{A}^{-1} \mathbf{d}$, which gives the explicit closed form in the statement.

Lemma 5. Assume the variance $\sigma^2 = 1$. Let $\eta, \xi > 0$, and k > 1. Suppose there are n control samples with Z = 0 at $x = -\xi$ and n treatment samples with Z = 1 at $x = \xi$; these form the overlap region. In addition, suppose there are kn control samples with Z = 0 at $x = -\xi - \eta$ and kn treatment samples with Z = 1 at $x = \xi + \eta$. These latter points are in the non-overlap region, and their distance η to the overlap region measures the level of overlap. Thus, the modulus of continuity is

$$\omega(\delta) := \frac{2k}{k+1} \max_{f \in \mathcal{F}_L, \sum_i f_{i,z_i}^2 \le \frac{\delta^2}{4}} \left[(f_{x_1,1} - f_{x_1,0}) + (f_{x_4,1} - f_{x_4,0}) \right].$$

Define the constants

$$\gamma := \frac{2}{n} \left(1 + \frac{1}{k} \right),$$

$$2kn$$

$$C := \frac{2kn}{k+1}L^2\eta^2,$$

$$\delta_c := \frac{2\sqrt{2nk(k+1)}}{k-1} L\eta,$$

$$s(\delta) := \sqrt{\frac{\delta^2}{4} - C}.$$

Then the worst-case bias and standard deviation of $\hat{\tau}_{\delta}$ are given by:

$$\overline{\text{bias}}(\hat{\tau}_{\delta}) = \begin{cases}
\frac{2L(2\xi + \eta)k}{k+1}, & \text{if } \delta \leq \delta_{c} \quad (i.e. \ L\eta \geq \frac{(k-1)\delta}{2\sqrt{2nk(k+1)}}), \\
k \left[\frac{2L(2\xi + \eta)}{(k+1)} + \frac{2(k-1)}{(k+1)^{2}} L\eta - \frac{C}{(k+1)} \frac{\sqrt{\frac{8}{n(k+1)}}}{s(\delta)} \right], & \text{if } \delta > \delta_{c} \quad (i.e. \ L\eta < \frac{(k-1)\delta}{2\sqrt{2nk(k+1)}}), \\
\text{sd}(\hat{\tau}_{\delta}) = \begin{cases}
\frac{k}{k+1} \sqrt{\frac{2}{n} \left(1 + \frac{1}{k}\right)}, & \text{if } \delta \leq \delta_{c}, \\
\frac{\sqrt{2}k}{(k+1)\sqrt{n(k+1)}} \frac{\delta}{s(\delta)}, & \text{if } \delta > \delta_{c}.
\end{cases}$$
(C.5)

Proof [Proof of Lemma 5] Let

$$x_1 = -\xi - \eta,$$
 $x_2 = -\xi,$ $x_3 = \xi,$ $x_4 = \xi + \eta.$

Write

$$a_i := f(x_i, 0), \qquad b_i := f(x_i, 1), \qquad i = 1, \dots, 4.$$

The distances between the points satisfy

$$|x_2 - x_1| = |x_4 - x_3| = \eta,$$
 $|x_3 - x_2| = 2\xi,$ $|x_4 - x_2| = 2\xi + \eta.$

We now consider the non-uniform quadratic weights

$$(n_1, n_2, n_3, n_4) = (kn, n, n, kn),$$

so that the quadratic constraint is

$$kn a_1^2 + n a_2^2 + n b_3^2 + kn b_4^2 \le \frac{\delta^2}{4}.$$
 (C.6)

The modulus of continuity for this configuration is

$$\omega(\delta) = \max_{f} \frac{2k}{k+1} \left[(f_{x_1,1} - f_{x_1,0}) + (f_{x_4,1} - f_{x_4,0}) \right]$$
$$= \max_{(a_i,b_i)} \frac{2k}{k+1} \left[(b_1 - a_1) + (b_4 - a_4) \right]$$

subject to the quadratic constraint (C.6) and the Lipschitz constraints

$$|a_i - a_j| \le L|x_i - x_j|, \qquad |b_i - b_j| \le L|x_i - x_j|, \qquad i \ne j.$$

Step 1: Reduction to a problem in v. Introduce

$$\mathbf{v} := (a_1, a_2, b_3, b_4)^{\top}, \qquad \mathbf{w} := (a_3, a_4, b_1, b_2)^{\top}.$$

The quadratic constraint (C.6) involves only v and can be written as

$$v^{\top}Qv \leq \frac{\delta^2}{4}, \qquad Q := \operatorname{diag}(kn, n, n, kn).$$

For each fixed \boldsymbol{v} , define

$$F(\boldsymbol{v}) := \max \left\{ (b_1 - a_1) + (b_4 - a_4) : (a_i, b_i) \text{ satisfy all Lipschitz constraints} \right\}. \tag{C.7}$$

Let

$$\mathcal{V} := \left\{ v : |a_1 - a_2| \le L\eta, \ |b_3 - b_4| \le L\eta \right\}. \tag{C.8}$$

These are exactly the Lipschitz conditions that involve only the coordinates in v. Then the original problem can be written as

$$\omega(\delta) = \frac{2k}{k+1} \max_{\boldsymbol{v} \in \mathcal{V}, \ \boldsymbol{v}^{\top} \boldsymbol{Q} \boldsymbol{v} \le \delta^2/4} F(\boldsymbol{v}). \tag{C.9}$$

Step 2: Remove redundant Lipschitz constraints. Assume $|a_1 - a_2| \le L\eta$. Suppose we choose a_3, a_4 such that

$$|a_3 - a_2| \le L(2\xi),$$

 $|a_4 - a_3| \le L\eta.$

Then all Lipschitz constraints for the a_i follow by the triangle inequality. Thus, conditional on $|a_1 - a_2| \le L\eta$, it suffices to enforce $|a_2 - a_3| \le L(2\xi)$ and $|a_3 - a_4| \le L\eta$.

Similarly, conditional on $|b_3 - b_4| \le L\eta$, it suffices to check the Lipschitz bounds $|b_3 - b_2| \le L(2\xi)$ and $|b_2 - b_1| \le L\eta$.

Step 3: Explicit computation of $F(\mathbf{v})$ (C.7). Fix $\mathbf{v} = (a_1, a_2, b_3, b_4)^{\top} \in \mathcal{V}$ (C.8).

We can verify that

$$a_4^{\star}(\mathbf{v}) = \min \left\{ a_4 : |a_2 - a_3| \le L(2\xi), |a_3 - a_4| \le L\eta \right\} = a_2 - L(2\xi + \eta),$$

and similarly.

$$b_1^{\star}(\boldsymbol{v}) = \max \{b_1 : |b_3 - b_2| \le L(2\xi), |b_2 - b_1| \le L\eta\} = b_3 + L(2\xi + \eta).$$

Combining the values of $a_4^{\star}(\mathbf{v})$ and $b_1^{\star}(\mathbf{v})$, we have

$$F(\mathbf{v}) = (b_1^* - a_1) + (b_4 - a_4^*)$$

= $(b_3 + L(2\xi + \eta) - a_1) + (b_4 - (a_2 - L(2\xi + \eta)))$
= $-a_1 - a_2 + b_3 + b_4 + 2L(2\xi + \eta).$

If we define

$$c := (-1, -1, 1, 1)^{\top},$$

then this can be written compactly as

$$F(\boldsymbol{v}) = \boldsymbol{c}^{\top} \boldsymbol{v} + 2L(2\xi + \eta).$$

From (C.9),

$$\omega(\delta) = \frac{2k}{k+1} \max_{\boldsymbol{v} \in \mathcal{V}, \ \boldsymbol{v}^{\top} \boldsymbol{Q} \boldsymbol{v} < \delta^2/4} (\boldsymbol{c}^{\top} \boldsymbol{v} + 2L(2\xi + \eta)). \tag{C.10}$$

Step 4: Solving the outer problem over v. The constant term $2L(2\xi + \eta)$ does not affect the optimizer, so we focus on maximizing $c^{\top}v$ subject to

$$oldsymbol{v}^{ op}oldsymbol{Q}oldsymbol{v} \leq rac{\delta^2}{4}, \qquad oldsymbol{v} \in \mathcal{V},$$

where \mathcal{V} is in (C.8). Let

$$Q^{-1} = \operatorname{diag}\left(\frac{1}{kn}, \frac{1}{n}, \frac{1}{n}, \frac{1}{kn}\right).$$

Introduce the vectors

$$\mathbf{h}_1 := (1, -1, 0, 0)^{\top}, \qquad \mathbf{h}_2 := (0, 0, 1, -1)^{\top},$$

so that $|a_1 - a_2| \leq L\eta$ and $|b_3 - b_4| \leq L\eta$ can be written as

$$|\boldsymbol{h}_1^{\top} \boldsymbol{v}| \leq L \eta, \qquad |\boldsymbol{h}_2^{\top} \boldsymbol{v}| \leq L \eta.$$

Define the scalars

$$\begin{split} \gamma &:= \boldsymbol{c}^{\top} \boldsymbol{Q}^{-1} \boldsymbol{c} = \frac{2}{n} \Big(1 + \frac{1}{k} \Big), \\ \beta &:= \boldsymbol{h}_{1}^{\top} \boldsymbol{Q}^{-1} \boldsymbol{h}_{1} = \boldsymbol{h}_{2}^{\top} \boldsymbol{Q}^{-1} \boldsymbol{h}_{2} = \frac{1}{n} \Big(1 + \frac{1}{k} \Big), \\ \alpha &:= \boldsymbol{h}_{1}^{\top} \boldsymbol{Q}^{-1} \boldsymbol{c} = \boldsymbol{h}_{2}^{\top} \boldsymbol{Q}^{-1} \boldsymbol{c} = \frac{1}{n} \Big(\frac{k-1}{k} \Big). \end{split}$$

Since we assume k > 1, we have $\alpha > 0$.

The quadratic program is

$$\max_{\boldsymbol{v} \in \mathbb{R}^4} \boldsymbol{c}^{\top} \boldsymbol{v} \quad \text{subject to} \quad \boldsymbol{v}^{\top} \boldsymbol{Q} \boldsymbol{v} \leq \frac{\delta^2}{4}, \qquad |\boldsymbol{h}_1^{\top} \boldsymbol{v}| \leq L \eta, \quad |\boldsymbol{h}_2^{\top} \boldsymbol{v}| \leq L \eta, \quad (C.11)$$

with $\mathbf{Q} = \operatorname{diag}(kn, n, n, kn)$, $\mathbf{c} = (-1, -1, 1, 1)^{\top}$, and $\mathbf{h}_1 = (1, -1, 0, 0)^{\top}$, $\mathbf{h}_2 = (0, 0, 1, -1)^{\top}$. Using a symmetry argument (as in the main text), we may assume that among the maximizers there exists \mathbf{v}^* such that $|\mathbf{h}_1^{\top} \mathbf{v}^*| = |\mathbf{h}_2^{\top} \mathbf{v}^*|$. For such an optimizer, either both Lipschitz constraints are slack $(|\mathbf{h}_1^{\top} \mathbf{v}^*| = |\mathbf{h}_2^{\top} \mathbf{v}^*| < L\eta)$, or both are binding $(|\mathbf{h}_1^{\top} \mathbf{v}^*| = |\mathbf{h}_2^{\top} \mathbf{v}^*| = L\eta)$. This yields the two regimes we analyze below.

Regime I: No Lipschitz constraints active.

Ignore the Lipschitz constraints and maximize $c^{\top}v$ over the ellipsoid $\{v: v^{\top}Qv \leq \delta^2/4\}$. Writing $w = Q^{1/2}v$ and $u = Q^{-1/2}c$, this becomes

$$\max_{\|\boldsymbol{w}\| \le \delta/2} \boldsymbol{u}^{\top} \boldsymbol{w},$$

whose maximizer is attained at $\mathbf{w}^* = (\delta/2) \mathbf{u}/\|\mathbf{u}\|$. Therefore

$$\max_{\boldsymbol{v}^{\top}\boldsymbol{Q}\boldsymbol{v}\leq\delta^{2}/4}\boldsymbol{c}^{\top}\boldsymbol{v} = \max_{\|\boldsymbol{w}\|\leq\delta/2}\boldsymbol{u}^{\top}\boldsymbol{w} = \frac{\delta}{2}\|\boldsymbol{u}\| = \frac{\delta}{2}\sqrt{\gamma}.$$

The corresponding optimizer (in v-coordinates) has

$$m{h}_1^{ op} m{v}_{
m unc}(\delta) = m{h}_2^{ op} m{v}_{
m unc}(\delta) = rac{\delta}{2} rac{lpha}{\sqrt{\gamma}}.$$

The Lipschitz constraints remain slack as long as $|\mathbf{h}_1^{\top} \mathbf{v}_{\text{unc}}(\delta)| \leq L\eta$, i.e.

$$\frac{\delta}{2} \frac{\alpha}{\sqrt{\gamma}} \le L\eta.$$

This defines the threshold

$$\delta_c := \frac{2L\eta\sqrt{\gamma}}{\alpha} = \frac{2\sqrt{2nk(k+1)}}{k-1}L\eta,$$

where we used the explicit expressions for γ and α and the assumption k > 1. For $0 \le \delta \le \delta_c$ the Lipschitz constraints do not bind and the unconstrained ellipsoid solution is feasible. Plugging $\mathbf{c}^{\top}\mathbf{v}_{\mathrm{unc}}(\delta) = (\delta/2)\sqrt{\gamma}$ into (C.10) yields

$$\omega(\delta) = \frac{2k}{k+1} \left(\frac{\delta}{2} \sqrt{\gamma} + 2L(2\xi + \eta) \right), \qquad 0 \le \delta \le \delta_c.$$
 (C.12)

Substituting $\gamma = \frac{2}{n} (1 + \frac{1}{k})$ gives the explicit Regime I expression.

Regime II: both Lipschitz constraints active. We now analyze the case where the quadratic constraint is loose enough that both Lipschitz constraints bind at the maximizer. From (C.11), we want to maximize $c^{\top}v$ subject to

$$\boldsymbol{v}^{\top} \boldsymbol{Q} \boldsymbol{v} \leq \frac{\delta^2}{4}, \qquad |\boldsymbol{h}_1^{\top} \boldsymbol{v}| \leq L \eta, \qquad |\boldsymbol{h}_2^{\top} \boldsymbol{v}| \leq L \eta.$$

By symmetry between the "left" and "right" coordinates, the maximizer must satisfy

$$\boldsymbol{h}_1^\top \boldsymbol{v} = \boldsymbol{h}_2^\top \boldsymbol{v} = L \eta.$$

Reformulation. Introduce the variables

$$w := Q^{1/2}v, \qquad u := Q^{-1/2}c,$$

so that

$$oldsymbol{c}^ op oldsymbol{v} = oldsymbol{u}^ op oldsymbol{w}, \qquad \|oldsymbol{w}\|^2 = oldsymbol{v}^ op oldsymbol{Q} oldsymbol{v} \leq rac{\delta^2}{4}.$$

Similarly, define

$$\boldsymbol{k}_j := \boldsymbol{Q}^{-1/2} \boldsymbol{h}_j, \quad j = 1, 2, \qquad K := [\boldsymbol{k}_1 \ \boldsymbol{k}_2] \in \mathbb{R}^{4 \times 2}, \qquad \boldsymbol{d}_{\text{vec}} := (L\eta, L\eta)^{\top}.$$

The Lipschitz equalities become

$$\boldsymbol{h}_j^{\top} \boldsymbol{v} = L \boldsymbol{\eta} \quad \Longleftrightarrow \quad \boldsymbol{k}_j^{\top} \boldsymbol{w} = L \boldsymbol{\eta} \quad \Longleftrightarrow \quad \boldsymbol{K}^{\top} \boldsymbol{w} = \boldsymbol{d}_{\text{vec}}.$$

Hence the Regime II problem is equivalent to

$$\max_{\boldsymbol{w} \in \mathbb{R}^4} \boldsymbol{u}^\top \boldsymbol{w} \quad \text{s.t.} \quad \|\boldsymbol{w}\|^2 \le \frac{\delta^2}{4}, \quad K^\top \boldsymbol{w} = \boldsymbol{d}_{\text{vec}}. \tag{C.13}$$

This is exactly of the form in Lemma 4 with m = 4, p = 2, \boldsymbol{u} as above, K as above, $\boldsymbol{d} = \boldsymbol{d}_{\text{vec}}$, and radius $R = \delta/2$. Lemma 4 therefore yields

$$\max \boldsymbol{u}^{\top} \boldsymbol{w} = \boldsymbol{b}^{\top} A^{-1} \boldsymbol{d}_{\text{vec}} + \sqrt{\gamma - \boldsymbol{b}^{\top} A^{-1} \boldsymbol{b}} \sqrt{\frac{\delta^{2}}{4} - \boldsymbol{d}_{\text{vec}}^{\top} A^{-1} \boldsymbol{d}_{\text{vec}}},$$
(C.14)

where

$$A := K^{\top} K, \qquad \boldsymbol{b} := K^{\top} \boldsymbol{u}, \qquad \gamma := \boldsymbol{u}^{\top} \boldsymbol{u} = \boldsymbol{c}^{\top} \boldsymbol{Q}^{-1} \boldsymbol{c}.$$

Explicit evaluation. From the definitions of h_1, h_2, Q and u, a direct computation shows

$$A = \begin{pmatrix} \beta & 0 \\ 0 & \beta \end{pmatrix}, \qquad \boldsymbol{b} = \begin{pmatrix} \alpha \\ \alpha \end{pmatrix},$$

with

$$\gamma = \frac{2}{n} \left(1 + \frac{1}{k} \right), \qquad \beta = \frac{1}{n} \left(1 + \frac{1}{k} \right), \qquad \alpha = \frac{1}{n} \left(\frac{k-1}{k} \right).$$

Using this structure,

$$\boldsymbol{b}^{\top} A^{-1} \boldsymbol{d}_{\text{vec}} = \frac{2\alpha L\eta}{\beta} = \frac{2(k-1)}{k+1} L\eta,$$

$$m{b}^{ op} A^{-1} m{b} = rac{2lpha^2}{eta} = rac{2(k-1)^2}{kn(k+1)}, \qquad m{d}_{ ext{vec}}^{ op} A^{-1} m{d}_{ ext{vec}} = rac{2(L\eta)^2}{eta} = rac{2kn}{k+1} L^2 \eta^2.$$

Moreover

$$\gamma - \frac{2\alpha^2}{\beta} = \frac{8}{n(k+1)}.$$

Plugging these into (C.14) yields

$$\max \mathbf{u}^{\top} \mathbf{w} = \frac{2(k-1)}{k+1} L \eta + \sqrt{\frac{8}{n(k+1)}} \sqrt{\frac{\delta^2}{4} - \frac{2kn}{k+1} L^2 \eta^2}.$$

Recalling that $c^{\top}v = u^{\top}w$ and substituting the above equation back into (C.10) gives the Regime II modulus

$$\omega(\delta) = \frac{2k}{k+1} \left(2L(2\xi + \eta) + \frac{2(k-1)}{k+1} L\eta + \sqrt{\frac{8}{n(k+1)}} \sqrt{\frac{\delta^2}{4} - \frac{2kn}{k+1} L^2 \eta^2} \right), \qquad \delta \ge \delta_c. \quad (C.15)$$

Combining the expressions from Regime I (C.12) and Regime II (C.15), we obtain the claimed piecewise closed-form expression for the modulus $\omega(\delta)$ with weights $(n_1, n_2, n_3, n_4) = (kn, n, n, kn)$.

Using (2.8), we have $\overline{\text{bias}}(\hat{\tau}_{\delta}) = \frac{1}{2}(\omega(\delta) - \delta\omega'(\delta))$. In addition, from (2.9), $\text{sd}(\hat{\tau}_{\delta}) = \omega'(\delta)$, and we finish the proof.

C.3 Derivation of the confidence sequence

Lemma 6. Fix $\alpha \in (0,1)$ and a sequence of nonnegative numbers $\{\alpha_t\}_{t\geq 1}$ such that

$$\sum_{t=1}^{\infty} \alpha_t \le \alpha.$$

For each $t \geq 1$, let τ_t denote the target estimand and write

$$\hat{\tau}_t = \tau_t + \text{bias}_t(f) + \text{sd}(\hat{\tau}_t) Z_t$$

where $Z_t \sim \mathcal{N}(0,1)$ and the bias satisfies

$$|\operatorname{bias}_t(f)| \leq \overline{\operatorname{bias}}(\hat{\tau}_t) \quad \text{for all } f \in \mathcal{F}.$$

Define the standardized worst-case bias

$$y_t := \frac{\overline{\operatorname{bias}}(\hat{\tau}_t)}{\operatorname{sd}(\hat{\tau}_t)}.$$

Let $\operatorname{cv}_{\alpha}(z)$ be the $(1-\alpha)$ -quantile of |N(z,1)|. Consider the confidence sequence

$$C_t := \hat{\tau}_t \pm \operatorname{sd}(\hat{\tau}_t) \operatorname{cv}_{\alpha_t}(y_t), \tag{C.16}$$

for $t = 1, 2, \dots$ Then

$$\inf_{f \in \mathcal{F}} \mathbb{P}_f (\forall t \ge 1: \ \tau_t \in \mathcal{C}_t) \ge 1 - \alpha.$$

In particular, the choice

$$\alpha_t := \frac{6\alpha}{\pi^2 t^2}$$

satisfies $\sum_{t=1}^{\infty} \alpha_t = \alpha$, and therefore $\{C_t\}_{t\geq 1}$ in (C.16) is an always-valid $(1-\alpha)$ confidence sequence.

Proof [Proof of Lemma 6] Fix an arbitrary data-generating function f and write \mathbb{P}_f for the corresponding probability measure. We will show that

$$\mathbb{P}_f(\forall t \geq 1: \ \tau_t \in \mathcal{C}_t) \geq 1 - \alpha,$$

and since f was arbitrary this implies the claimed uniform bound over f.

For each $t \geq 1$, define the failure event

$$F_t := \{ \tau_t \notin \mathcal{C}_t \} = \{ |\hat{\tau}_t - \tau_t| > \operatorname{sd}(\hat{\tau}_t) \operatorname{cv}_{\alpha_t}(y_t) \}.$$

By the decomposition

$$\hat{\tau}_t - \tau_t = \text{bias}_t(f) + \text{sd}(\hat{\tau}_t) Z_t$$

on F_t we have

$$\left|\operatorname{bias}_{t}(f) + \operatorname{sd}(\hat{\tau}_{t}) Z_{t}\right| > \operatorname{sd}(\hat{\tau}_{t}) \operatorname{cv}_{\alpha_{t}}(y_{t}).$$

Dividing by $sd(\hat{\tau}_t)$ and setting

$$\mu_t(f) := \frac{\operatorname{bias}_t(f)}{\operatorname{sd}(\hat{\tau}_t)},$$

we can write

$$F_t = \{ |Z_t + \mu_t(f)| > \operatorname{cv}_{\alpha_t}(y_t) \}, \qquad |\mu_t(f)| \le y_t,$$

where the last inequality uses the bias bound $|\text{bias}_t(f)| \leq \text{bias}(\hat{\tau}_t)$.

By the definition of $\operatorname{cv}_{\alpha_t}(z)$, for every $z \geq 0$ and every $|\mu| \leq z$,

$$\mathbb{P}(|N(\mu, 1)| > \operatorname{cv}_{\alpha_t}(z)) \le \alpha_t.$$

Applying this with $z = y_t$ and $\mu = \mu_t(f)$ shows that

$$\mathbb{P}_f(F_t) = \mathbb{P}_f(|Z_t + \mu_t(f)| > \operatorname{cv}_{\alpha_t}(y_t)) \le \alpha_t \quad \text{for all } t \ge 1.$$
 (C.17)

Now consider the event that the confidence sequence ever fails:

$$F := \left\{ \exists t \ge 1 : \ \tau_t \notin \mathcal{C}_t \right\} = \bigcup_{t=1}^{\infty} F_t.$$

By the union bound and (C.17),

$$\mathbb{P}_f(F) = \mathbb{P}_f\left(\bigcup_{t=1}^{\infty} F_t\right) \le \sum_{t=1}^{\infty} \mathbb{P}_f(F_t) \le \sum_{t=1}^{\infty} \alpha_t \le \alpha.$$

Therefore

$$\mathbb{P}_f(\forall t \ge 1: \ \tau_t \in \mathcal{C}_t) = 1 - \mathbb{P}_f(F) \ge 1 - \alpha.$$

Since this holds for every f, taking the infimum over f completes the proof.

D Experimental details

D.1 Details of Example 1

First, we provide additional details and analysis of Example 1. We let $\mathbb{P}(Z=1|X=x)=\pi(x)$ given in (D.1), and we also set the true outcome function to be $f(x,z)=F(x)+\mathcal{I}(z=1)\cdot h(x)$ given by (D.2). Both $\pi(x)$ and f(x,z) are parameterized by two parameters: κ and η that govern the size of the limited overlap region. A smaller κ and η means the limited overlap region is smaller, while H controls the value of the ATE τ . Given the true outcome function, we generate data $y_i = f(x_i, z_i) + \epsilon_i$ where $\epsilon_i \sim N(0, \sigma^2)$ with $\sigma = 0.06$. Despite the low noise, we see the unreliability of typical asymptotic estimators. We take $\kappa = 0.05, \eta = 0.05, H = 0.25$ unless specified otherwise.

$$\pi(x) = \begin{cases} \frac{\kappa}{\eta} x, & \text{if } 0 \le x \le \eta, \\ -\frac{\kappa}{\eta} (x - \eta) + (1 - \kappa), & \text{if } \eta < x \le 2\eta, \\ \frac{1 - 2\kappa}{1 - 2\eta} (x - 2\eta) + \kappa, & \text{if } x > 2\eta, \end{cases}$$
(D.1)

$$h(x) = 8H\left(x - \frac{1}{2}\right)^{2}, \quad F(x) = \begin{cases} \frac{4H}{\eta^{2}}\left(x - \frac{\eta}{2}\right)^{2} + H, & \text{if } 0 \leq x \leq \frac{\eta}{2}, \\ -\frac{4H}{\eta^{2}}x(x - \eta), & \text{if } \frac{\eta}{2} < x \leq \eta, \\ 32H\left(x - \eta\right)\left(x - \eta - \frac{1}{2}\right), & \text{if } \eta < x \leq \eta + \frac{1}{2}, \\ -\frac{16H}{(2\eta - 1)^{2}}\left(x - \eta - \frac{1}{2}\right)(x - 1), & \text{if } \eta + \frac{1}{2} < x \leq 1. \end{cases}$$
(D.2)

We simulate n=1000 points of X according to the data-generating process described above. As discussed, for AlPW_{partial}, after truncation, one needs to analyze the ATE in the non-overlap region τ_{-} (2.14), and our minimax approach MP can build a minimax CI that guarantees coverage of τ_{-} . On the other hand, as we see earlier in Figure 10, the naive minimax approach M does not fully exploit the data in the overlap region and produces an overly conservative interval that is driven by the worst-case bias of the ATE applied on the entire data.

D.2 Details of the case study in Section 4

We first present a lemma that allows us to generate an observational dataset given a propensity score function from a randomized controlled trial (RCT) dataset. We treat the ATE estimated from the RCT dataset as the ground truth treatment effect and generate observational datasets using the approach described in Lemma 7.

Lemma 7. Let the dataset be $\mathcal{D} = \{x_i, y_i, z_i\}_{i=1}^n$ and assume $z_i \sim \text{Bernoulli}(p)$ for some $p \in (0, 1)$. For every i, let $C_i \sim \text{Bernoulli}(\pi(x_i))$. Define a random variable O as follows: if $p \leq \frac{1}{2}$, then

$$O_i := \begin{cases} 1 & \text{if } z_i = 1, \\ \text{Bernoulli}(\frac{p}{1-p}) & \text{if } z_i = 0, \end{cases}$$

and if $p > \frac{1}{2}$, let

$$O_i := \begin{cases} 1 & \text{if } z_i = 0, \\ \text{Bernoulli}(\frac{1-p}{p}) & \text{if } z_i = 1. \end{cases}$$

And let $I_i = \mathcal{I}\left(z_i = C_i \text{ and } O_i = 1\right)$. We define another dataset \mathcal{D}' as

$$\mathcal{D}' := \{x_i, y_i, z_i\}_{i \in \{j \in [n]: I_j = 1\}},$$

then $P(z_i = 1 | I_i = 1) = \pi(x_i)$ so that \mathcal{D}' is an observational dataset with propensity score π . In addition, we have $\mathbb{P}(I_i = 1) = \min\{p, 1 - p\}$.

Proof [Proof of Lemma 7] We assume $p \leq \frac{1}{2}$ (the other case can be proved similarly). Then we have

$$\mathbb{P}(I_i = 1 | z_i = 1) = \mathbb{P}(O_i = 1 | z_i = 1) \cdot \mathbb{P}(C_i = 1) = \pi(x_i),$$

$$\mathbb{P}(I_i = 1 | z_i = 0) = \mathbb{P}(O_i = 1 | z_i = 0) \cdot \mathbb{P}(C_i = 0) = \frac{p}{1 - p}(1 - \pi(x_i)),$$

so that

$$\mathbb{P}(I_i = 1) = \mathbb{P}(I_i = 1 | z_i = 1) \mathbb{P}(z_i = 1) + \mathbb{P}(I_i = 1 | z_i = 0) \mathbb{P}(z_i = 0) = p\pi(x_i) + (1 - p) \frac{p}{1 - p} (1 - \pi(x_i)) = p,$$

$$\mathbb{P}(z_i = 1 | I_i = 1) = \frac{\mathbb{P}(I_i = 1 | z_i = 1) \mathbb{P}(z_i = 1)}{\mathbb{P}(I_i = 1)} = \frac{p\pi(x_i)}{p} = \pi(x_i),$$

and we finish the proof.

We now describe the propensity score we use. We first use the entire RCT dataset to train a lightgbm regressor to estimate the conditional treatment effect $\tilde{\tau}(x)$, then construct the propensity score $\pi(x)$ based on the quantile of $\tilde{\tau}(x)$, see (4.1).

D.3 Experimental results for continual sampling

We use the same data as in Section 5.1. Using the confidence sequence (5.3), we simulate the confidence sequence assuming the analyst can sample 6 epochs of new data

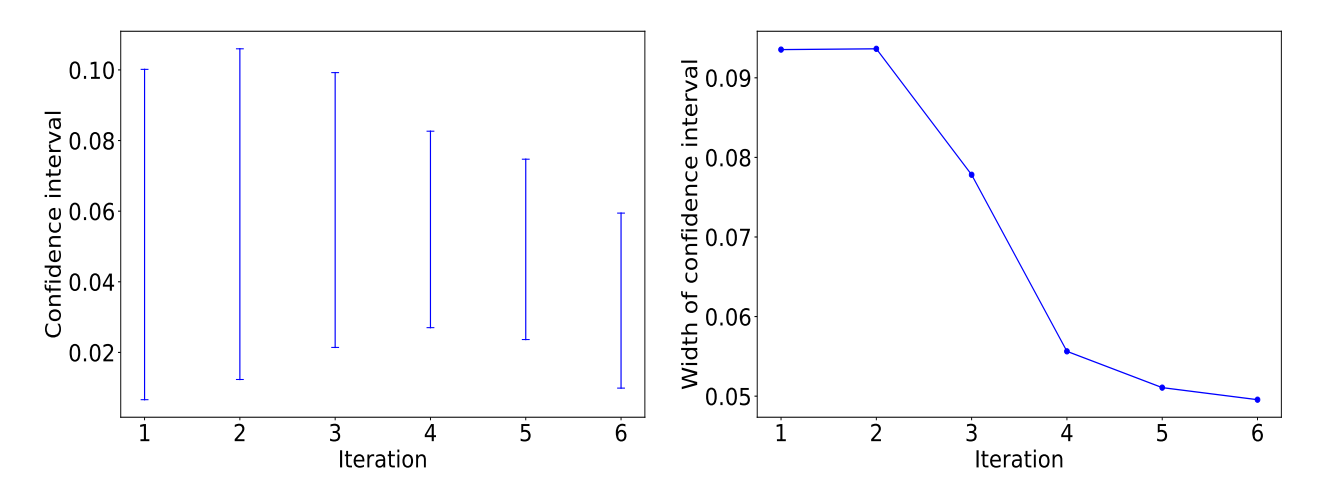


Figure 16: A confidence sequence generated during continual sampling

 $(x \in (0.40, 0.47), (0.47, 0.53), (0.53, 0.60), (0, 0.03), (0.03, 0.07), (0.07, 0.10))$ in the non-overlap region with a fixed truncation threshold and L = 5.48. From Figure 16, we observe that the length of the confidence interval decreases and that the interval becomes closer to the origin as the number of iterations increases, indicating that the uncertainty over the non-overlap region gradually decreases.